

# **SUPPORTING INFORMATION**

## **Interpreting Hydrogen-Deuterium Exchange Events in Proteins Using Atomistic Simulations: Case Studies on Regulators of G-protein Signaling Proteins**

Hossein Mohammadiarani,<sup>†,¶</sup> Vincent S. Shaw,<sup>‡,¶</sup> Richard R. Neubig,<sup>‡</sup> and Harish  
Vashisth<sup>\*,†</sup>

<sup>†</sup>*Department of Chemical Engineering, University of New Hampshire, Durham, NH 03824,  
United States, and* <sup>‡</sup>*Department of Pharmacology and Toxicology, Michigan State University,  
East Lansing, MI 48825, United States*

E-mail: harish.vashisth@unh.edu

Phone: (603)-862-2483. Fax: (603)-862-3747

---

\*To whom correspondence should be addressed

<sup>†</sup>University of New Hampshire, Durham, NH, USA

<sup>‡</sup>Michigan State University, East Lansing, MI, USA

<sup>¶</sup>co-first authors

# Table of Contents

Supplemental Introduction .....	S5
Supplemental Methods .....	S8

## List of Tables

S1 Summary of simulations .....	S8
S2 Models proposed in this work .....	S10
S3 Default and optimized parameter values for all models .....	S13

## List of Figures

S1 Experimentally-measured deuterium incorporation in RGS proteins .....	S11
S2 Fragment definition for each RGS protein .....	S12
S3 DI in RGS4 (PDB:1AGR, AMBER, default parameters) .....	S14
S4 DI in RGS4 (PDB:1EZT, AMBER, default parameters) .....	S15
S5 DI in RGS8 (PDB:2IHD, AMBER, default parameters) .....	S16
S6 DI in RGS8 (PDB:2ODE, AMBER, default parameters) .....	S17
S7 DI in RGS19 (PDB:1CMZ, AMBER, default parameters) .....	S18
S8 DI in RGS4 (PDB:1AGR, AMBER, optimized parameters) .....	S19
S9 DI in RGS4 (PDB:1EZT, AMBER, optimized parameters) .....	S20
S10 DI in RGS8 (PDB:2IHD, AMBER, optimized parameters) .....	S21
S11 DI in RGS8 (PDB:2ODE, AMBER, optimized parameters) .....	S22
S12 DI in RGS19 (PDB:1CMZ, AMBER, optimized parameters) .....	S23
S13 DI in RGS4 (PDB:1AGR, AMBER, new models) .....	S24
S14 DI in RGS4 (PDB:1EZT, AMBER, new models) .....	S25
S15 DI in RGS8 (PDB:2IHD, AMBER, new models) .....	S26

S16	DI in RGS8 (PDB:2ODE, AMBER, new models)	S27
S17	DI in RGS19 (PDB:1CMZ, AMBER, new models)	S28
S18	DI in RGS4 (PDB:1AGR, CHARMM, default parameters)	S29
S19	DI in RGS4 (PDB:1EZT, CHARMM, default parameters)	S30
S20	DI in RGS8 (PDB:2IHD, CHARMM, default parameters)	S31
S21	DI in RGS8 (PDB:2ODE, CHARMM, default parameters)	S32
S22	DI in RGS19 (PDB:1CMZ, CHARMM, default parameters)	S33
S23	DI in RGS4 (PDB:1AGR, CHARMM, optimized parameters)	S34
S24	DI in RGS4 (PDB:1EZT, CHARMM, optimized parameters)	S35
S25	DI in RGS8 (PDB:2IHD, CHARMM, optimized parameters)	S36
S26	DI in RGS8 (PDB:2ODE, CHARMM, optimized parameters)	S37
S27	DI in RGS19 (PDB:1CMZ, CHARMM, optimized parameters)	S38
S28	DI in RGS4 (PDB:1AGR, CHARMM, new models)	S39
S29	DI in RGS4 (PDB:1EZT, CHARMM, new models)	S40
S30	DI in RGS8 (PDB:2IHD, CHARMM, new models)	S41
S31	DI in RGS8 (PDB:2ODE, CHARMM, new models)	S42
S32	DI in RGS19 (PDB:1CMZ, CHARMM, new models)	S43
S33	DI mapping on RGS structures at t = 1000 (experiment vs. modeling)	S44
S34	RMSF of each RGS simulation	S45
S35	Modeled deuterium incorporation at 1000 minute (RGS4, CHARMM)	S46
S36	Modeled deuterium incorporation at 1000 minute (RGS8, CHARMM)	S46
S37	Modeled deuterium incorporation at 1000 minute (RGS4, AMBER)	S47
S38	Modeled deuterium incorporation at 1000 minute (RGS8, AMBER)	S47
S39	Modeled deuterium incorporation at 1000 minute (RGS19, CHARMM)	S48
S40	Modeled deuterium incorporation at 1000 minute (RGS19, AMBER)	S48
S41	Snapshots of salt-bridges in RGS proteins	S49
S42	SASA of amide hydrogens	S50

S43	Corrected mean residence time for amide hydrogens	S51
S44	Correlation of open states using model M7 (RGS4, PDB:1AGR, CHARMM)	S52
S45	Correlation of open states using model M7 (RGS8, PDB:2ODE, CHARMM)	S53
S46	Probability of opening transitions in amides	S54

# Supporting Information

## Supplemental Introduction

In the following, we provide details on seven existing models for protection factor (PF) correlations, as shown in Table 1 of the main article.

Model M1: Resing et al.<sup>1</sup> conducted early studies to predict exchange rates in a kinase protein (ERK2) by fitting protection factors to an equation of the form  $\log(PF_i) = \log(k_{int}/k_{hdX}) = u * (SA_i) + v/(HB_i)$ , where  $k_{hdX}$  is the experimentally measured exchange rate of an amide hydrogen,  $k_{int}$  is the intrinsic exchange rate calculated according to Bai et al.,<sup>2</sup>  $SA_i$  is the distance of each amide hydrogen from the surface of protein in Å, and  $HB_i$  is the hydrogen-bond length of backbone amide nitrogens to an acceptor. They also used deuterium exchange rates measured by Milne et al.<sup>3</sup> for horse heart cytochrome c.

Model M2: Vendruscolo et al.<sup>4</sup> proposed a model for predictions of HDX rates based on the exploration of conformations using Monte Carlo (MC) sampling biased by experimental data. They speculated that the protection of amide hydrogens comes from buried part of the amide group and also from the hydrogen bonding in the secondary structure which resulted in a phenomenological expression including the number of contacts of residue  $i$  with other residues ( $N_i^c$ ) and the number of hydrogen bonds formed by the amide hydrogens of residues ( $N_i^h$ ), respectively. According to their definition, hydrogen bonds are present if the angle between the NH vector and the OH vector is below 0.7 rad and the OH distance is below 2.4 Å. Also, two residues are in contact if any pair of their atoms are closer than 8.5 Å.

Model M3: Best et al.<sup>5</sup> used the same phenomenological expression that Vendruscolo et al.<sup>4</sup> had proposed but with minor changes in definition of  $N_i^c$  and  $N_i^h$ . The contribution of burial in the model is the number of heavy atoms within a distance of 6.5 Å from the amide nitrogen. A cutoff of 2.4 Å between the donor hydrogen and the acceptor was used for identifying a hydrogen bond without an angle criterion. They optimized the parameters of their model using experimental protection factors and the corresponding protection factors from a 1 ns conventional MD simulation

of seven different proteins. They acknowledge that major protein fluctuations were elusive from short MD simulations that motivated them to conduct a biased simulation of the protein bovine pancreatic trypsin inhibitor (BPTI) by using hydrogen-exchange restraints with varying values of the parameters.

Model M4: Kieseritzky et al.<sup>6</sup> used MD simulations as a complement for hydrogen exchange experiments. They simulated oxidized c-type cytochrome under native conditions (PDB code 1K3H) with the CHARMM22 force-field using explicit water molecules modeled using the TIP3P water model. The simulation was 3 ns long. They proposed a protection factor definition based on a linear combination of protection factors  $\log(PF_i) = \log(k_{int}/k_{hdX}) = \beta_1 PFE_1 + \beta_2 PFE_2$ . They optimized parameters  $\beta_1$  and  $\beta_2$  to arrive at an agreement between computed (based on MD simulation data) and measured hydrogen exchange protection factors. The nine different protection factor correlations in their paper show varieties of error and Pearson's correlation coefficient out of which  $PFE_1$  = [the number of residues which are in contact with corresponding residue] and  $PFE_2$  = [the inverse of the backbone atom RMSF] show the least error and the best correlation.

Model M5: A model was suggested by Ma et al.<sup>7</sup> where  $NH_i^\beta$  is the average number of hydrogen bonds between the NH atom of residue  $i$  and C=O backbone oxygen within 2.6 Å distance, and  $NH_i^{sol}$  is the average number of hydrogen bonds between NH and water oxygen within 3.0 Å distance of residue  $i$ . In the original model,  $NH_\beta$  is measured in  $\beta$ -sheets and the correlation is marginal  $PF_i = (NH_i^{sol} + NH_i^\beta) / C.NH_i^{sol}$ . They used CHARMM27 force-field to do MD simulations of different  $\beta$ -sheet conformations, each of which was for 60 ns.

Model M6: Park et al.<sup>8</sup> recently developed a novel model based on a comprehensive HDX-MS experimental data using Amber 11 ff99SB force-field and a 100 ns long simulation. Their logistics growth function HDX model consist of one fitting parameter called "base".  $NHstat_i$  is defined as ([the number of snapshots showing H-bonding of amide hydrogen to protein]-[the number of snapshots showing H-bonding amide hydrogen to water ])/[the total number of snapshots]. They provided three amide hydrogen-bond models out of which model HB2 has been compared with other models in their work. In the HB2 model, H-bonding of a given amide hydrogen to the side-

chain as well as C=O group in the backbone are counted as H-bonding of amide hydrogens to protein. The fraction of deuterium incorporation (DI) for each amide hydrogen was computed by the first order reaction kinetics  $DI_i^{res} = 1 - \exp(-k_{int,it}/PF_i)$ .

Model M7: Persson et al.<sup>9</sup> used a significantly long MD simulation of protein BPTI (0.262 ms long) generated by Shaw et al.<sup>10</sup> using Amber ff99SB-I/TIP4P-Ew force-field. They start with a description of the standard model in which each amide can be exposed to solvent in an open state or buried within the protein by a closed state:  $(N-H)_c \xrightleftharpoons[k_o]{k_c} (N-H)_o \xrightarrow{k_{int}} (N-D)_o$  in which HDX rate is given as  $k_{hdx} = k_o k_{int} / (k_o + k_c + k_{int})$ . The assumption of  $k_{int} \ll k_c + k_o$ , which is an applicable assumption for HDX experiment, results in a simple and practical phenomenological model  $k_{hdx} = k_{int} / (PF + 1)$ . The protection factor here is the key for the calculation of hydrogen-deuterium exchange rate and it is defined as the ratio of residence time in the closed state to residence time in the open-state which is applicable to MD simulations. The criteria for the open state and the closed state play an important role in computing protection factors. They speculate that a direct access to external solvent and disruption of any intramolecular H-bond with the N-H group are key factors in defining the open-state. A residue is in an open state when the amide hydrogen has at least two water oxygens within 2.6 Å and that the amide hydrogen has no other polar protein atoms (except in neighboring residues) within 2.6 Å.

Other studies: In addition to models highlighted above, Craig et al.<sup>11</sup> modeled deuterium incorporation of three different proteins using coarse-grained MD simulations. The open state criteria were evaluated by the number of contacts per residue and the distance changes between the H-bonded residues compared to their native conformations. Pertuk et al.<sup>12</sup> studied a kinase protein (ERK2MAP) using all-atom explicit-water MD simulations and showed that both the whole dynamically averaged solvent accessible surface area (SASA) and the number of waters in the first solvation shell of each amide nitrogen can be used as metrics for predicting deuterium incorporation. Recently, Adhikary et al.<sup>13</sup> have modeled deuterium incorporation using multiple MD simulations (each 450-ns long) of neurotransmitter sodium symporters.

## Supplemental Methods

### System setup: MD simulations

A summary of all MD simulations for RGS4, RGS8, and RGS19 is provided in Table S1. Specifically, 10 independent MD simulations, each 2  $\mu$ s long, were conducted using both CHARMM and AMBER force-fields for all apo-RGS proteins.

**Table S1: A summary of all MD simulations.**

Protein	PDB	system-size (atoms)	force-field (trajectory length)
RGS4	1AGR	28160	CHARMM36 (2 $\mu$ s), AMBER (2 $\mu$ s)
	1EZT	29275	CHARMM36 (2 $\mu$ s), AMBER (2 $\mu$ s)
RGS8	2IHD	27490	CHARMM36 (2 $\mu$ s), AMBER (2 $\mu$ s)
	2ODE	30731	CHARMM36 (2 $\mu$ s), AMBER (2 $\mu$ s)
RGS19	1CMZ	29560	CHARMM36 (2 $\mu$ s), AMBER (2 $\mu$ s)

### Protocols for HDX Modeling

The HDX-MS experiments provided fragment-based DI whereas in MD simulations, it is feasible to calculate DI at a residue resolution. In Figure S2, we show details on all fragments and their residues for RGS4, RGS8, and RGS19. To compare DI between experiments and simulations, DI of residues (except Prolines that do not have amide hydrogens) were averaged over the corresponding fragment using Eq. (1).

$$DI_i^{\text{frag}} = \frac{\sum_{j=1, \neq \text{PRO}}^m DI_j^{\text{res}}}{m}; \text{ where } m \text{ is the number of residues in the fragment.} \quad (1)$$

For all models, we calculated the intrinsic HDX kinetic rates per Bai et al.<sup>2</sup> at 273 K, the temperature at which our HDX-MS experiments were conducted. Initially, we analyzed 100,000 frames for each 2  $\mu$ s MD trajectory by applying the default criteria reported in the literature for models M1 through M7 to compute PFs of amides for all RGS proteins. We then re-optimized the parameters of all models by minimizing an objective function (Eq. (2)) which incorporates HDX-



MS data and MD simulations of all RGS proteins. It should be noted here that the optimization of parameters were carried out separately for each force-field due to the fact that CHARMM and AMBER force-fields are parameterized differently for studies of protein dynamics.

$$\text{OF} = \sum_{\text{SYS}=1}^5 \left( \sum_{\text{frag}=1}^n \left| \text{DI}_{\text{exp}}^{\text{frag}} - \text{DI}_{\text{sim}}^{\text{frag}} \right| \right)_{\text{SYS}} \quad (2)$$

where OF is the objective function, DI is deuterium incorporation, SYS is the number of simulations for an RGS protein using the same force-field, and *frag* is the fragment number. All default and re-optimized parameters of models M1 through M7 are listed in Table S3.

**New HDX models M8 and M9 proposed in this work:** In addition to existing models (M1-M7), we revisited and evaluated SASA of amide hydrogens as a metric in prediction of amide PFs because contradictory observations regarding the use of SASA as a metric have been proposed in the literature. Published studies indicate that SASA of amide hydrogens reasonably predicts the number of exchanged hydrogens<sup>12</sup> or is an even better indicator for protected hydrogens than using H-bonds.<sup>14</sup> Contrary to this view, a lack of agreement between HDX experiments and MD simulations based on SASA has been reported.<sup>9</sup> Besides, although anticorrelations between the SASA of amide hydrogens and the residue-resolution protection factors from experiments existed, Park et al.<sup>8</sup> chose H-bonds as a metric for HDX modeling to overcome the limitation of using SASA and they concluded that H-bonds are a generic and suitable metric for the estimation of PFs.

We therefore developed two new models (listed as M8 and M9 in Table S2 and Table S3) using the distances of amide hydrogens from the first polar atom as an alternative metric along with SASA of each amide hydrogen to comply with the theory of HDX in which a residue may be protected by polar atoms despite having large enough SASA.<sup>9,15</sup> This assertion comes from the fact that surface exposed hydrogens (with higher values of SASA) can be significantly protected from hydrogen exchange.<sup>1</sup> Surprisingly, these two metrics in combination have resulted in trends and values consistent with experiments.

Specifically, model M8 is an empirical model (similar to models M1 through M6) based upon SASA of amide hydrogens and distances of amide hydrogens to the first polar atom (except in the

**Table S2: Models proposed in this work.**

Model	Protection factor criteria
M8	$\ln(PF_i) = (\beta_s SASA_i^{-\gamma_s} + \beta_p D_i^{-\gamma_p})$
M9	$PF_i = \tau_C / \tau_O$

neighboring residues) ( $D_i$ ) and  $\ln(PF_i)$  is a power function of  $SASA_i$  and  $D_i$ . However, model M9 is a fractional population model<sup>9</sup> where the same metrics ( $SASA_i$  and  $D_i$ ) were used for distinguishing between the open and closed states of amides. We define the open state in model M9 for each amide hydrogen when its SASA crosses a threshold value ( $d_{sasa}$ ) and that the amide hydrogen has no other polar protein atom (except in neighboring residues) within a threshold distance ( $d_p$ ). The values of thresholds/cut-offs in model M9 and four correlation coefficients in model M8 are obtained by minimizing the objective function in Eq. (2). The intrinsic exchange rates in new models were also calculated according to Bai et al.<sup>2</sup>

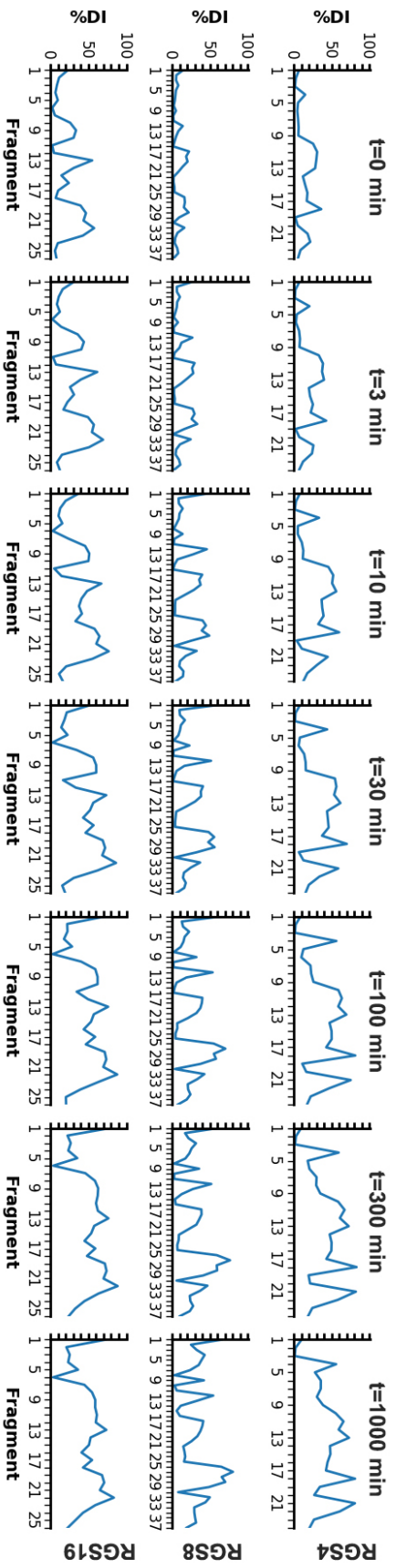


Figure S1: Experimentally measured percentage deuterium incorporation (%DI) of fragments in RGS proteins at  $t = 0, 3, 10, 30, 100, 300,$  and  $1000$  minutes (RGS4: top row; RGS8: middle row; RGS19: bottom row).

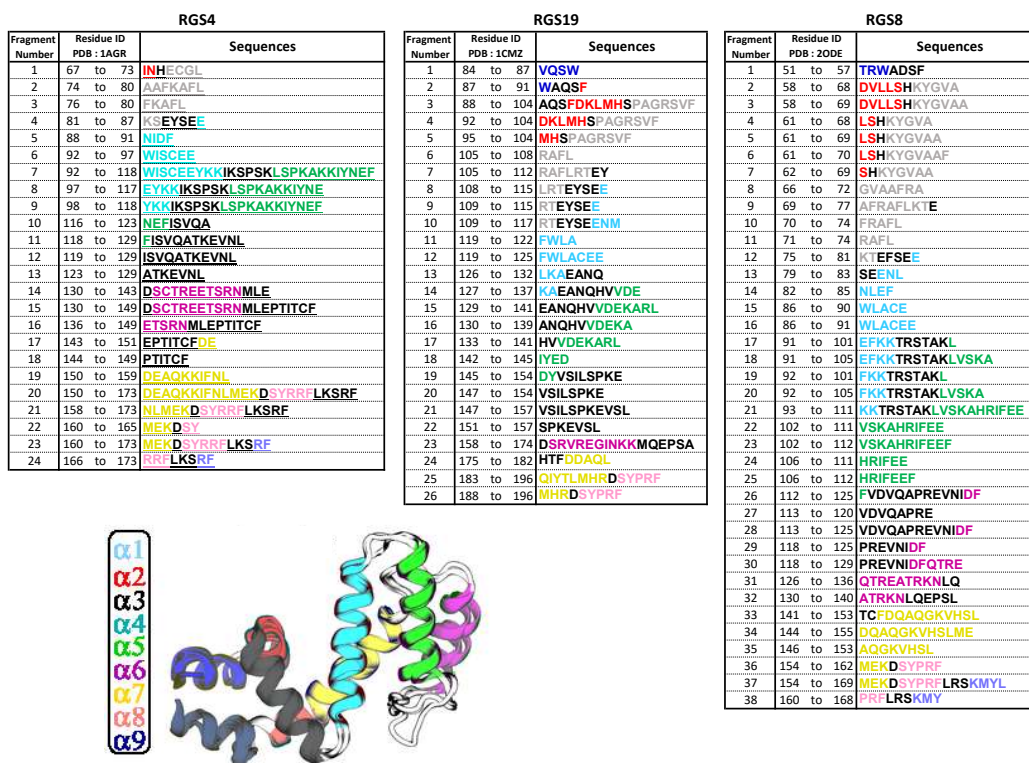


Figure S2: Definitions of fragments for each RGS protein. Each fragment comprises residues whose color determines their location in nine  $\alpha$ -helices of each RGS protein. Residue names in connecting loops are highlighted in black, but shown as white cartoons in the protein structure. All helices are colored and labeled in the protein rendering.

**Table S3: Details on all protection-factor correlation models with the default and re-optimized values of their parameters. Optimized values based upon simulations conducted using CHARMM and AMBER force-fields are listed with superscripts *ch* and *am*, respectively. In addition, details on two new models M8 and M9 proposed in this work are listed.**

	Model	Criteria	
Literature	M1 <sup>1</sup> (1999–resing)	$\log(PF_i) = u(SA_i) + v/(HB_i)$ $u = 0.76, v = 8.2$ $u^{ch} = 6.15, v^{ch} = 5.32$ $u^{am} = 5.18, v^{am} = 4.92$	
	M2 <sup>4</sup> (2003–Vendruscolo)	$\ln(PF_i) = (\beta_c N_i^c + \beta_h N_i^h)$ $\beta_c = 1, \beta_h = 5$ $\beta_c^{ch} = 0.49, \beta_h^{ch} = 0.85$ $\beta_c^{am} = 0.5, \beta_h^{am} = 0.9$	
	M3 <sup>5</sup> (2006–Best)	$\ln(PF_i) = (\beta_c N_i^c + \beta_h N_i^h)$ $\beta_c = 0.35, \beta_h = 2$ $\beta_c^{ch} = 0.23, \beta_h^{ch} = 5.40$ $\beta_c^{am} = 0.23, \beta_h^{am} = 4.00$	
	M4 <sup>6</sup> (2006–Kieseritzky)	$\ln(PF_i) = (\beta_c N_i^c + \beta_r (N_i^r)^{-1})$ $\beta_c = 0.5, \beta_r = 0.9$ $\beta_c^{ch} = 0.45, \beta_r^{ch} = 1.31$ $\beta_c^{am} = 0.19, \beta_r^{am} = 6.45$	
	M5 <sup>7</sup> (2011–Ma)	$PF_i = (C_o NH_i^{sol} + C_c NH_i^\beta) / C_o NH_i^{sol}$ $C_o^{ch} = 8.48e^{-6}, C_c^{ch} = 2.50$ $C_o^{am} = 0.15, C_c^{am} = 1.47e^4$	
	M6 <sup>8</sup> (2015–Park)	$PF_i = base / (1 + (\sqrt{base})^{1-NH_{stat_i}})$ $base = 10^8$ $base^{ch} = 1.3e^8$ $base^{am} = 0.4e^8$	
	M7 <sup>9</sup> (2015–Persson)	$PF_i = \tau_C / \tau_O$ $d_w = 2.6 \text{ \AA}, d_p = 2.6 \text{ \AA}$ $d_w^{ch} = 2.43 \text{ \AA}, d_p^{ch} = 2.73 \text{ \AA}$ $d_w^{am} = 2.40 \text{ \AA}, d_p^{am} = 2.73 \text{ \AA}$	
	This work	M8	$\ln(PF_i) = (\beta_s SASA_i^{-\gamma_s} + \beta_p D_i^{-\gamma_p})$ $\beta_s^{ch} = 0.72, \beta_p^{ch} = 2.60e^1$ $\gamma_s^{ch} = 0.53, \gamma_p^{ch} = 0.99$ $\beta_s^{am} = 1.30e^{-3}, \beta_p^{am} = 3.65e^1$ $\gamma_s^{am} = 2.64, \gamma_p^{am} = 1.27$
		M9	$PF_i = \tau_C / \tau_O$ $d_{sasa}^{ch} = 9.15 \text{ \AA}^2, d_p^{ch} = 3.00 \text{ \AA}$ $d_{sasa}^{am} = 8.02 \text{ \AA}^2, d_p^{am} = 2.99 \text{ \AA}$

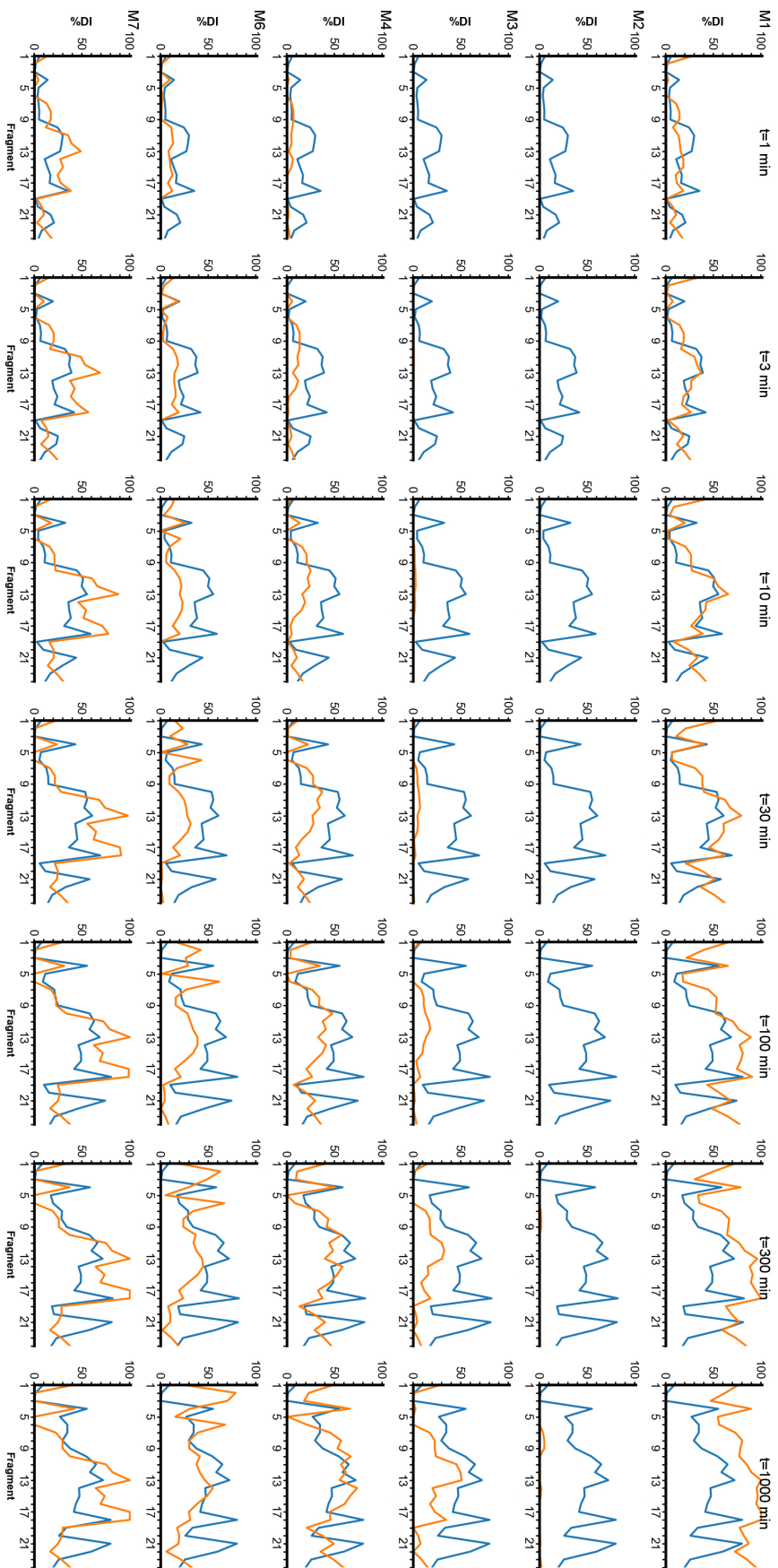


Figure S3: Deuterium incorporation of fragments in RGS4 . The HDX experiment (blue) and different models with default parameters (red) are shown in seven discrete times. This figure shows the MD simulation results for PDB:1AGR and AMBER Force-field.

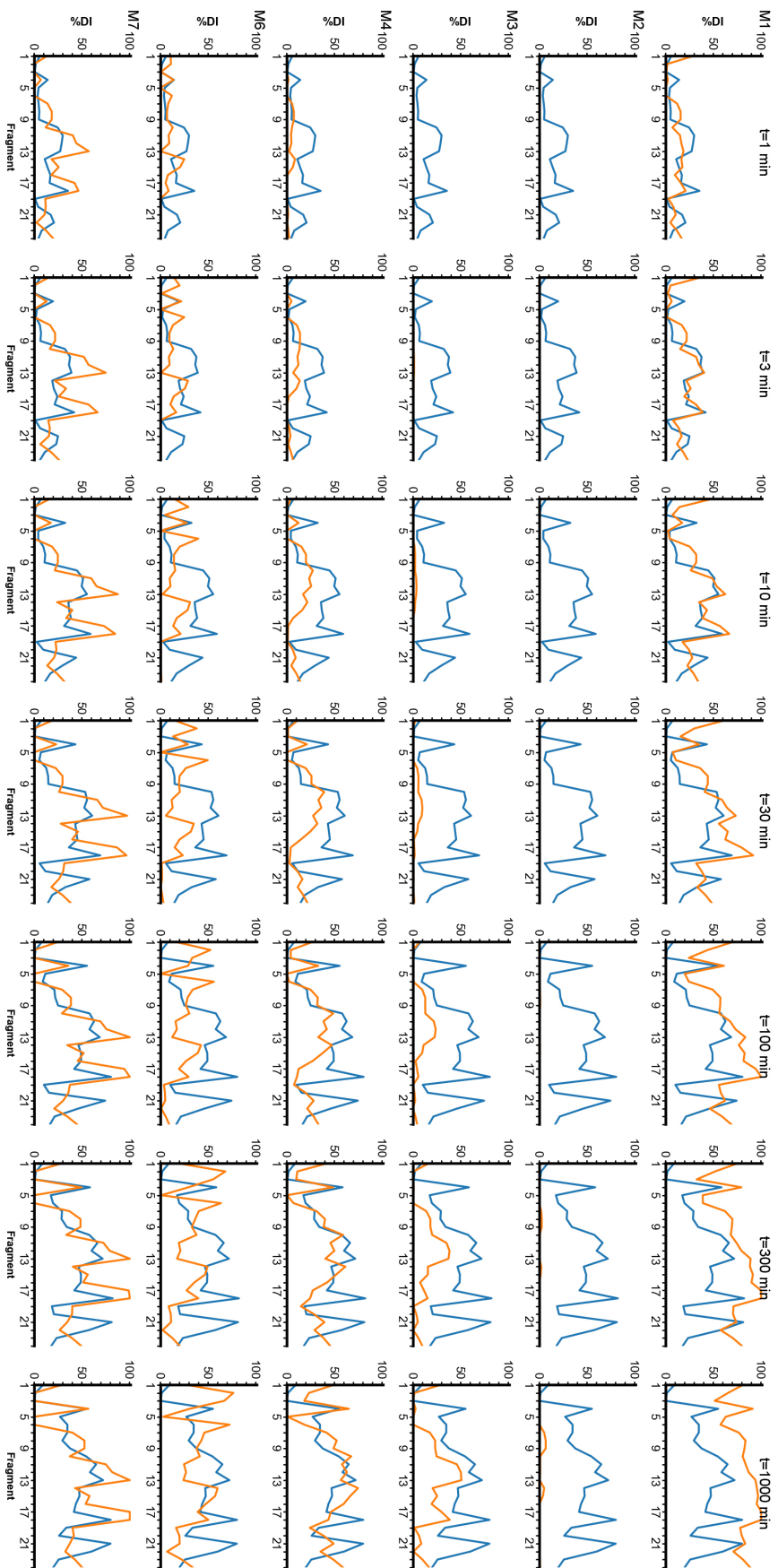


Figure S4: Deuterium incorporation of fragments in RGS4. The HDX experiment (blue) and different models with default parameters (red) are shown in seven discrete times. This figure shows the MD simulation results for PDB:1E7T and AMBER Force-field.

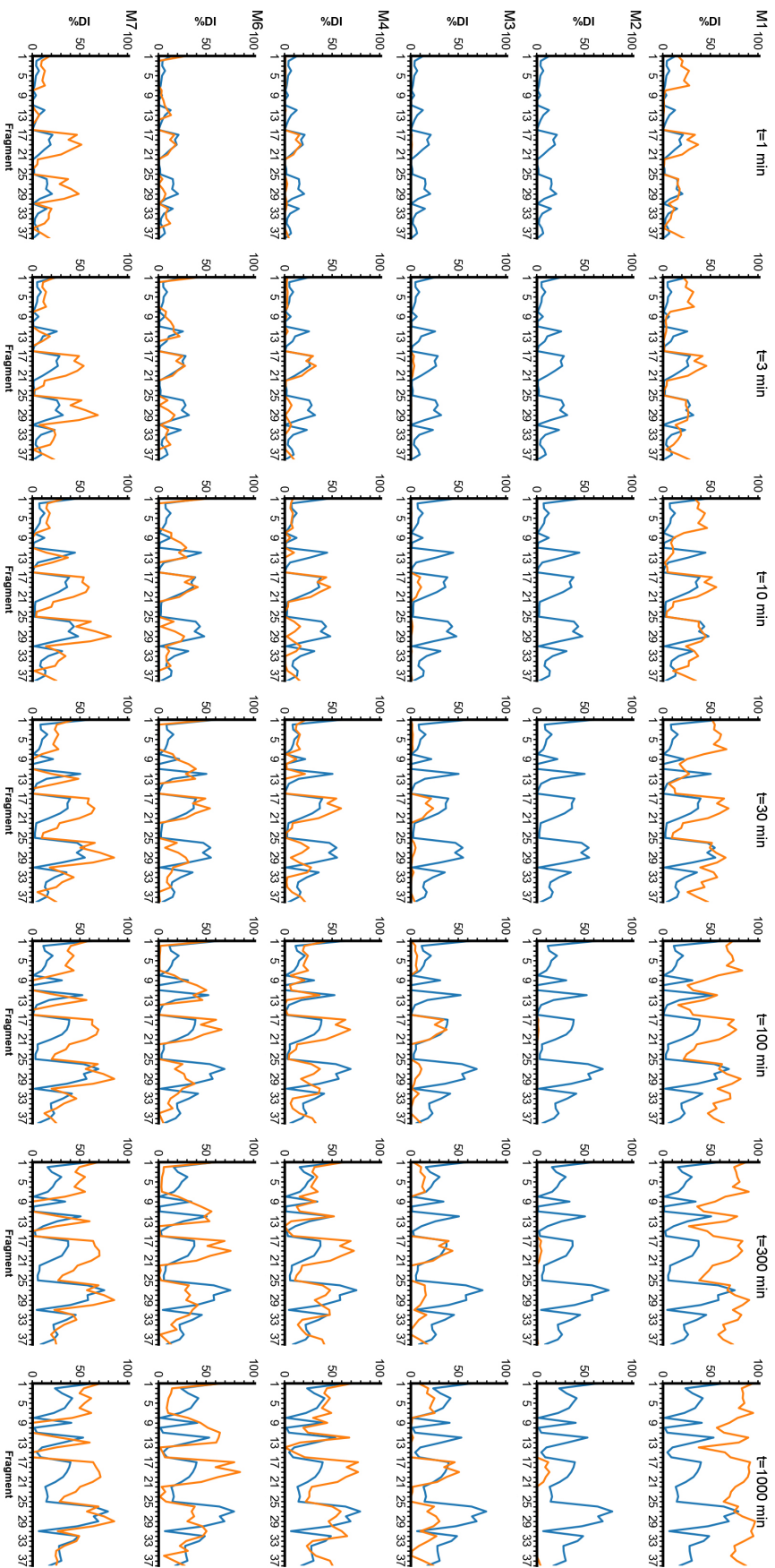


Figure S5: Deuterium incorporation of fragments in RGS8. The HDX experiment (blue) and different models with default parameters (red) are shown in seven discrete times. This figure shows the MD simulation results for PDB:2IHD and AMBER Force-field.



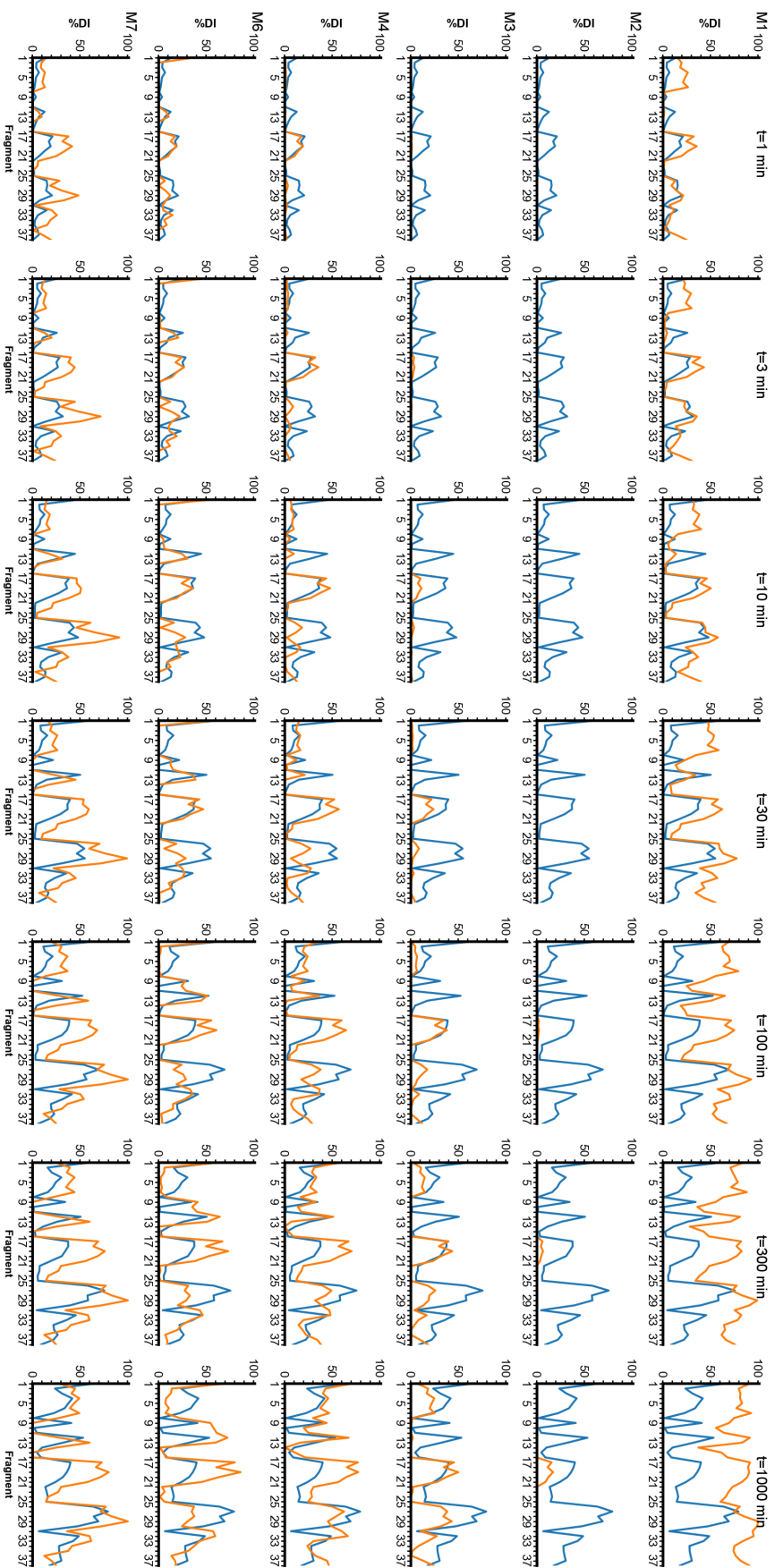


Figure S6: Deuterium incorporation of fragments in RGS8. The HDX experiment (blue) and different models with default parameters (red) are shown in seven discrete times. This figure shows the MD simulation results for PDB:2ODE and AMBER Force-field.

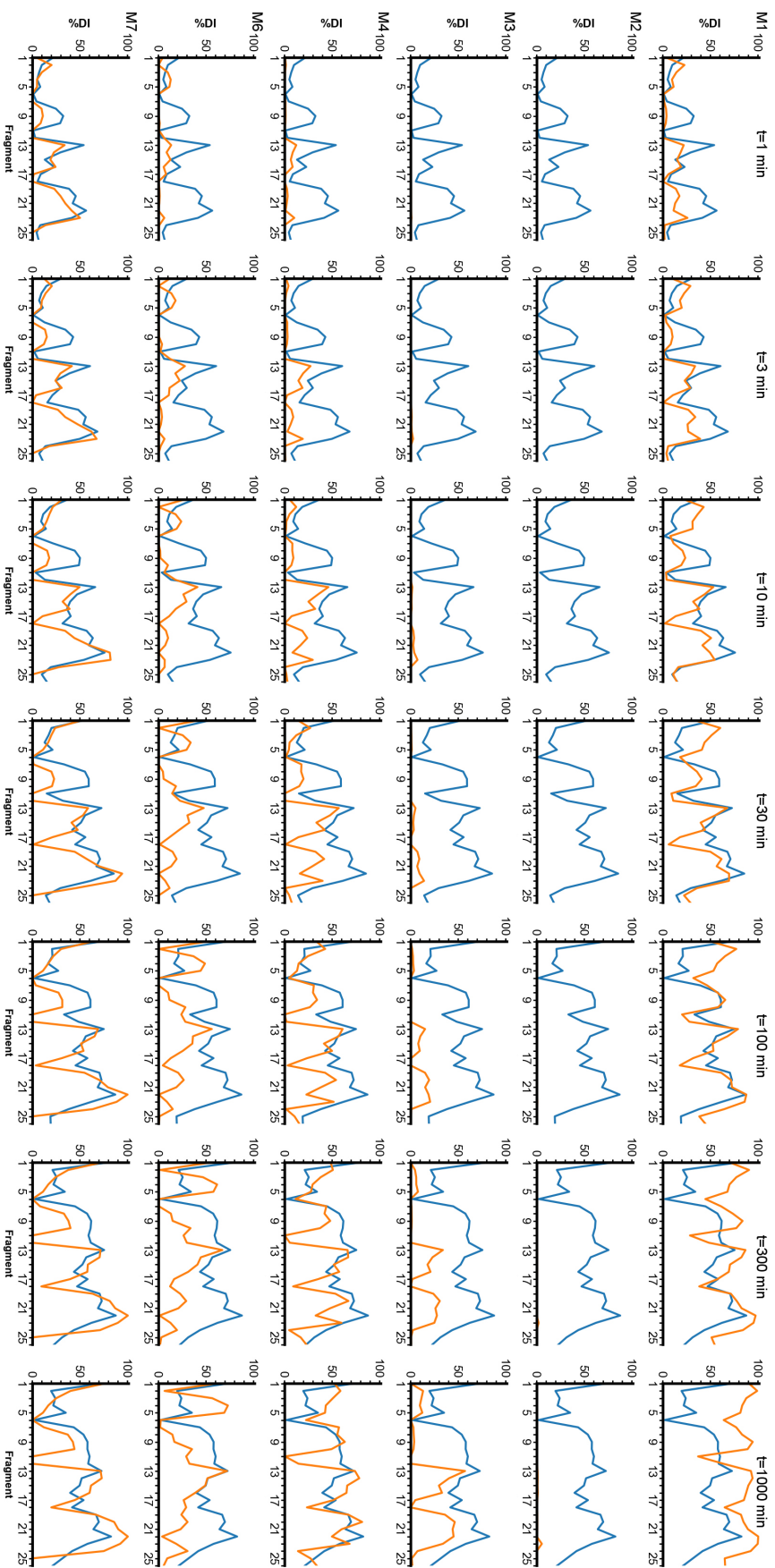


Figure S7: Deuterium incorporation of fragments in RGS19. The HDX experiment (blue) and different models with default parameters (red) are shown in seven discrete times. This figure shows the MD simulation results for PDB:1CMZ and AMBER Force-field.

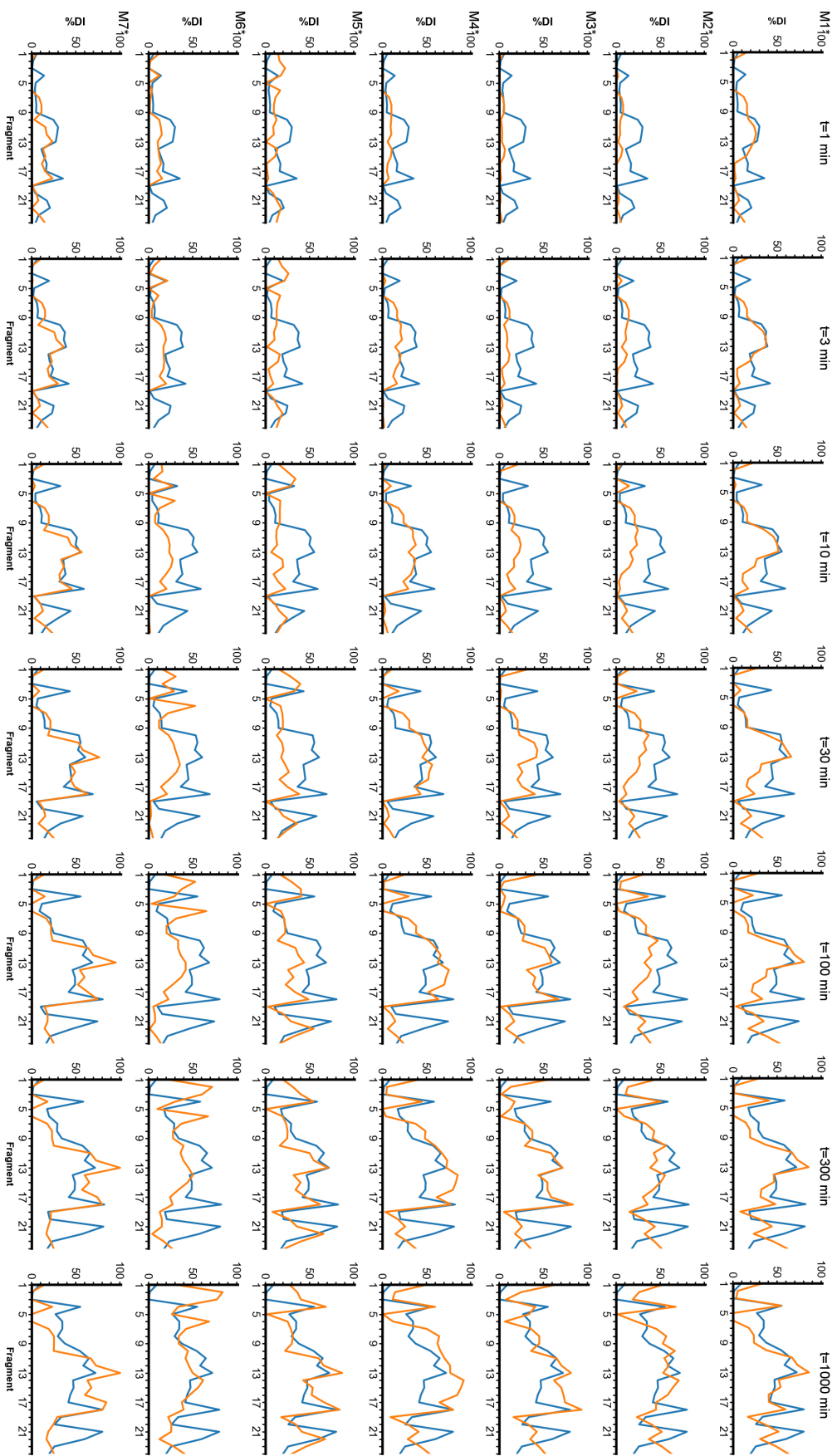


Figure S8: Deuterium incorporation of fragments in RGS4 in RGS4. The HDX experiment (blue) and different models with optimized parameters (red) are shown in seven discrete times. This figure shows the MD simulation results for PDB:1AGR and AMBER Force-field.

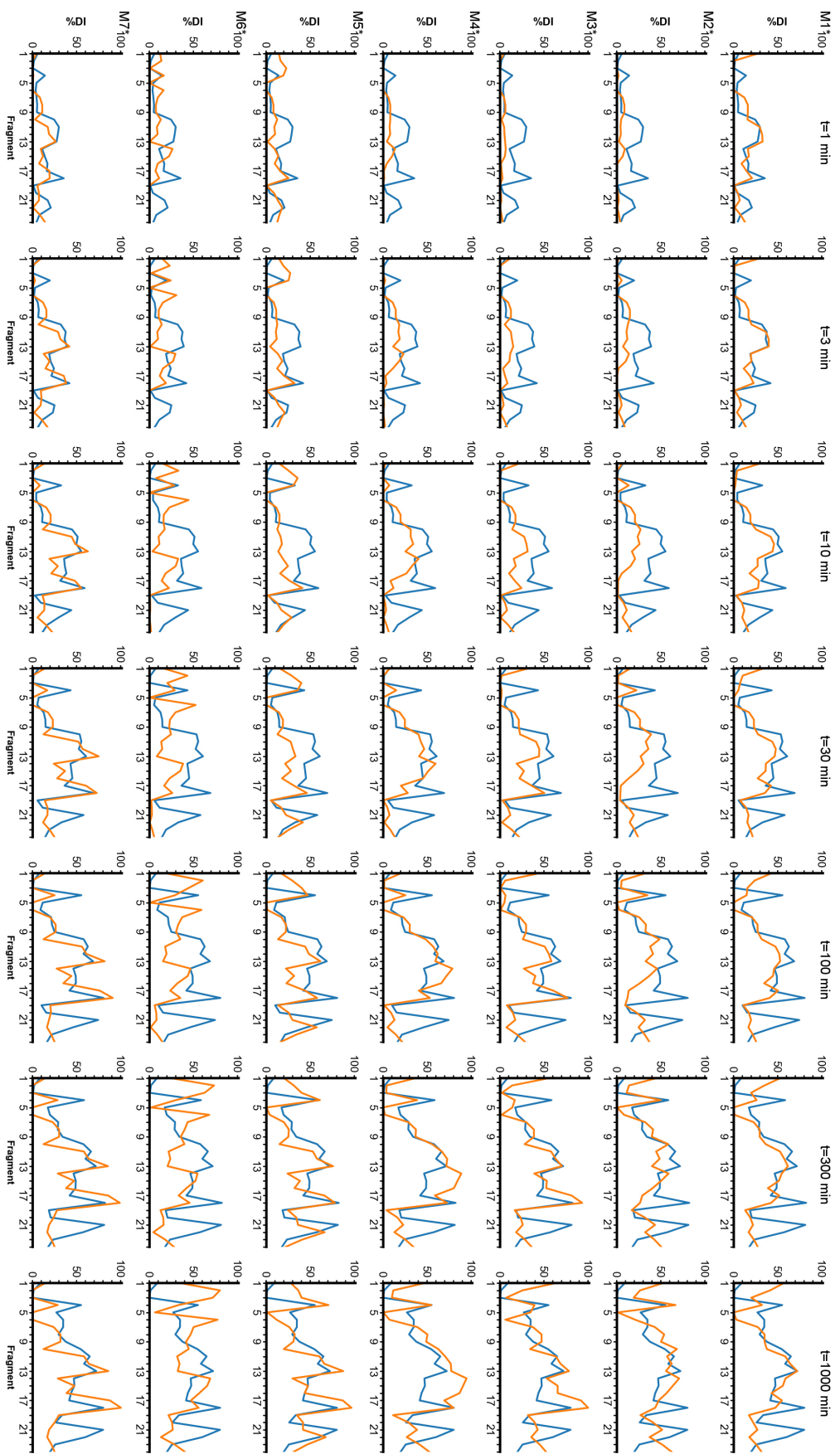


Figure S9: Deuterium incorporation of fragments in RGS4. The HDX experiment (blue) and different models with optimized parameters (red) are shown in seven discrete times. This figure shows the MD simulation results for PDB: 1EZT and AMBER Force-field.

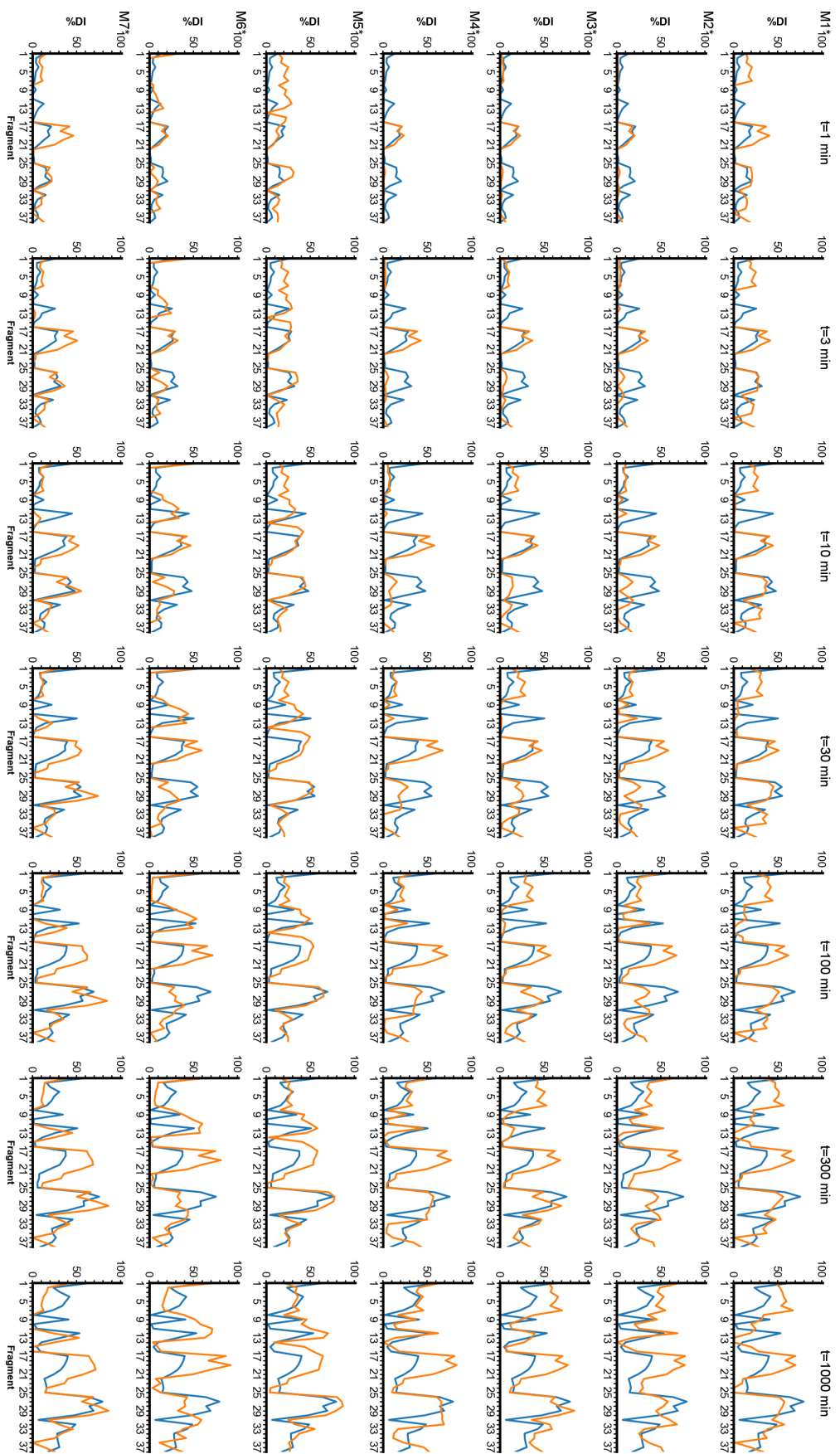


Figure S10: Deuterium incorporation of fragments in RGS8. The HDX experiment (blue) and different models with optimized parameters (red) are shown in seven discrete times. This figure shows the MD simulation results for PDB:2IHD and AMBER Force-field.

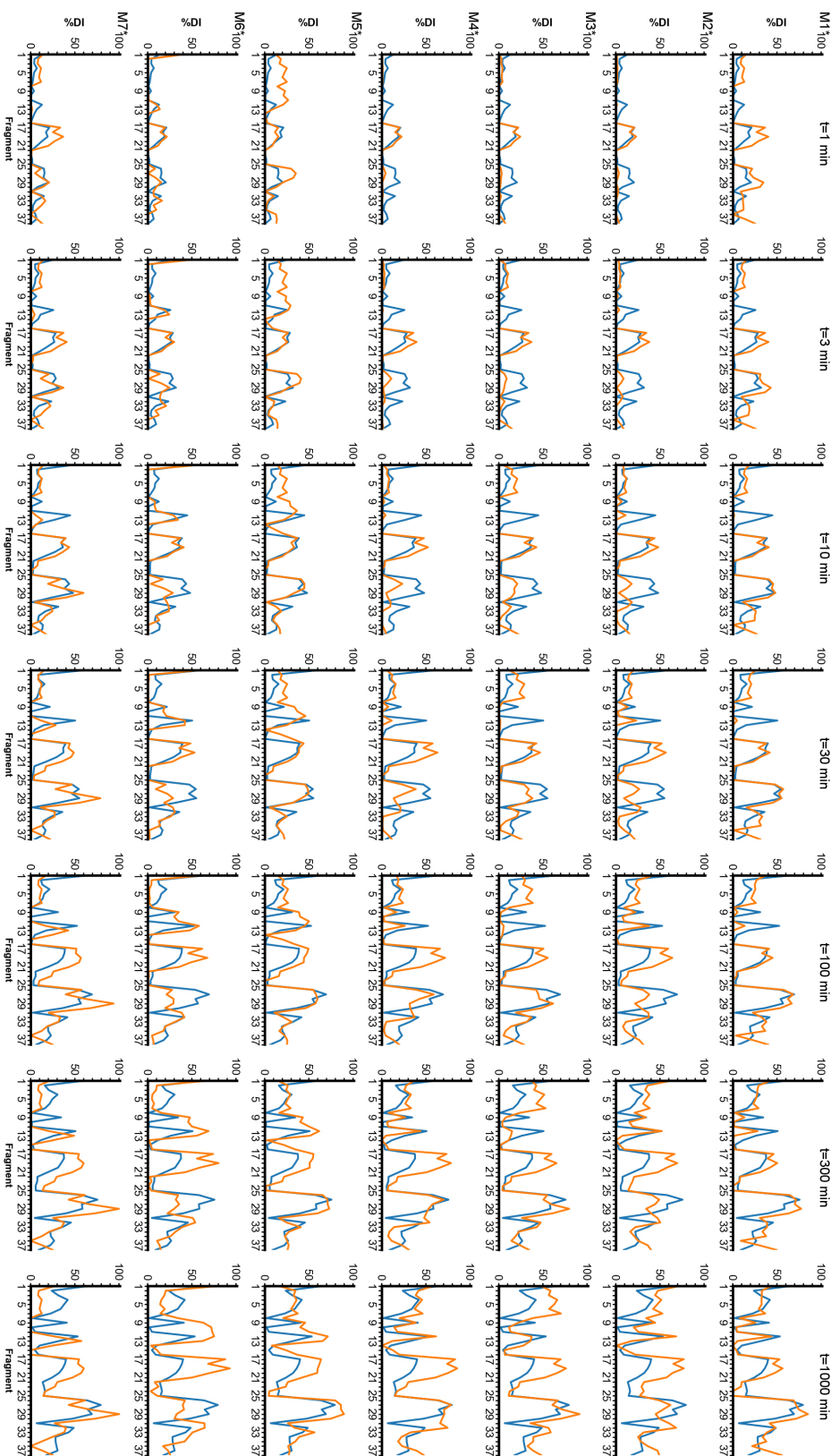


Figure S11: Deuterium incorporation of fragments in RGS8. The HDX experiment (blue) and different models with optimized parameters (red) are shown in seven discrete times. This figure shows the MD simulation results for PDB:2ODE and AMBER Force-field.

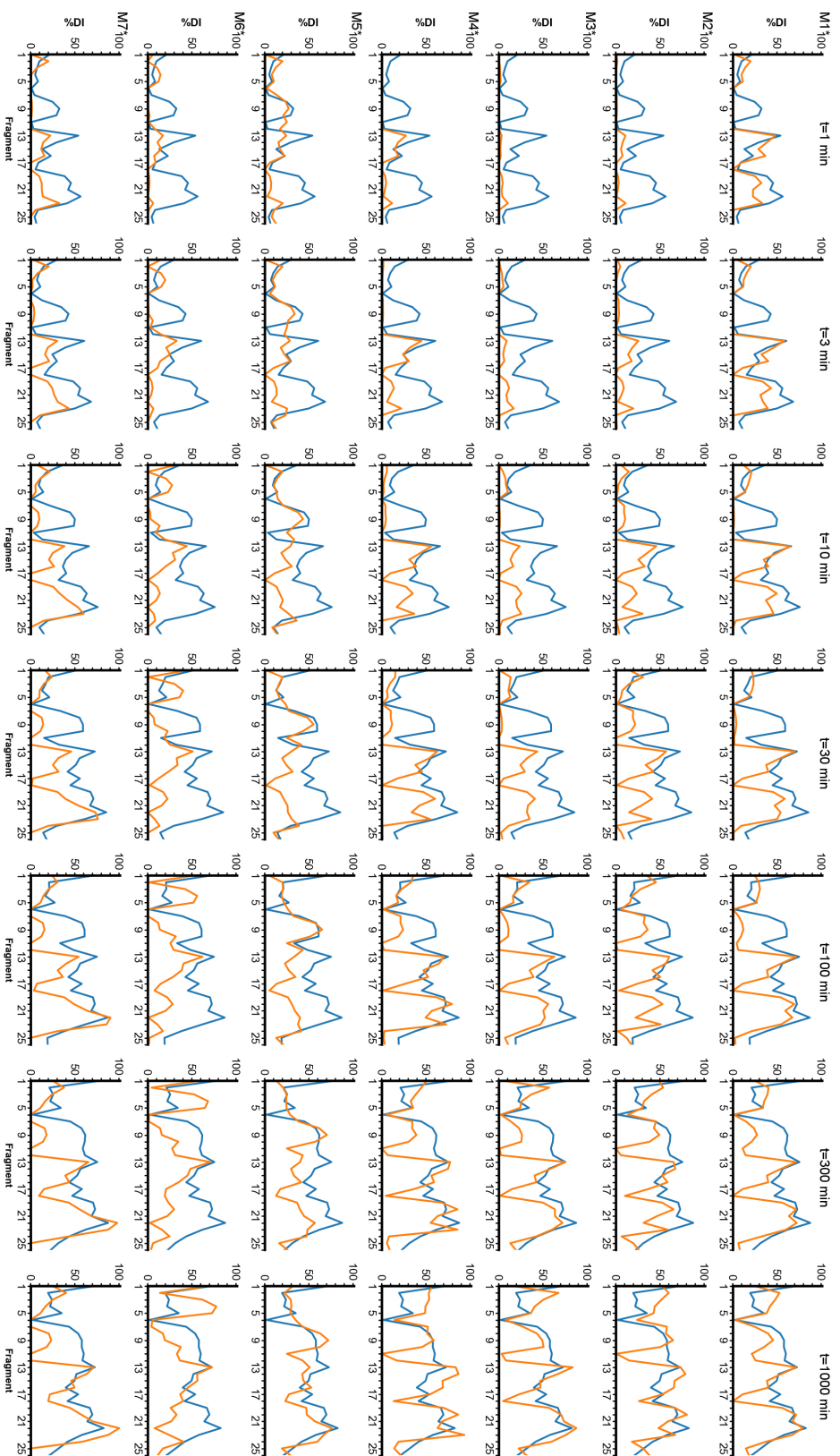


Figure S12: Deuterium incorporation of fragments in RGS19. The HDX experiment (blue) and different models with optimized parameters (red) are shown in seven discrete times. This figure shows the MD simulation results for PDB:1CMZ and AMBER Force-field.

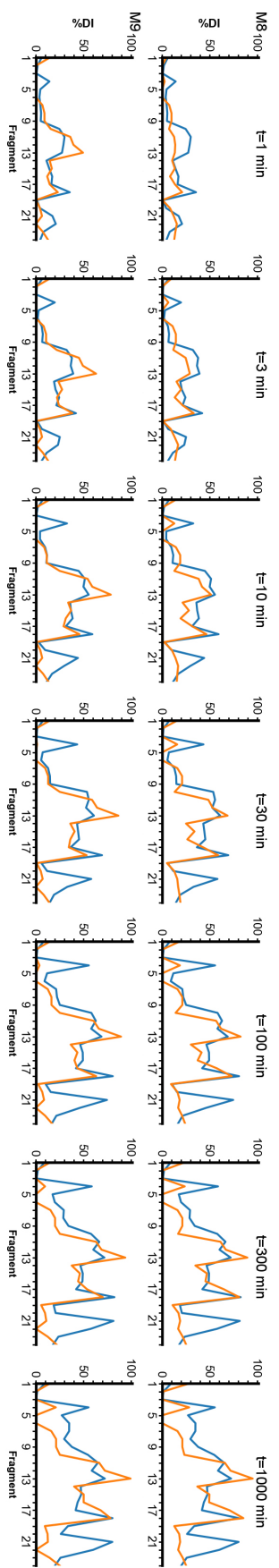


Figure S13: Deuterium incorporation of fragments in RGS4. The HDX experiment (blue) and the new models (M8, M9) with optimized parameters (red) are shown in seven discrete times. This figure shows the MD simulation results for PDB:1AGR and AMBER Force-field.



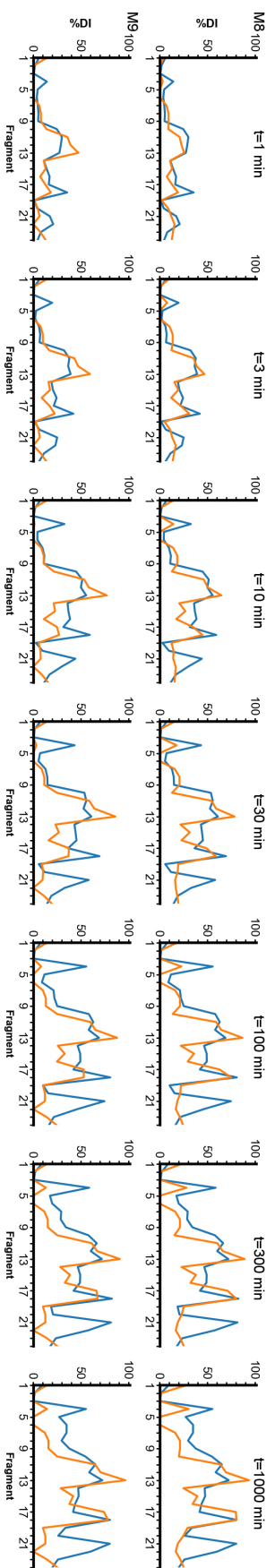


Figure S14: Deuterium incorporation of fragments in RGS4. The HDX experiment (blue) and the new models (M8, M9) with optimized parameters (red) are shown in seven discrete times. This figure shows the MD simulation results for PDB:1EZT and AMBER Force-field.

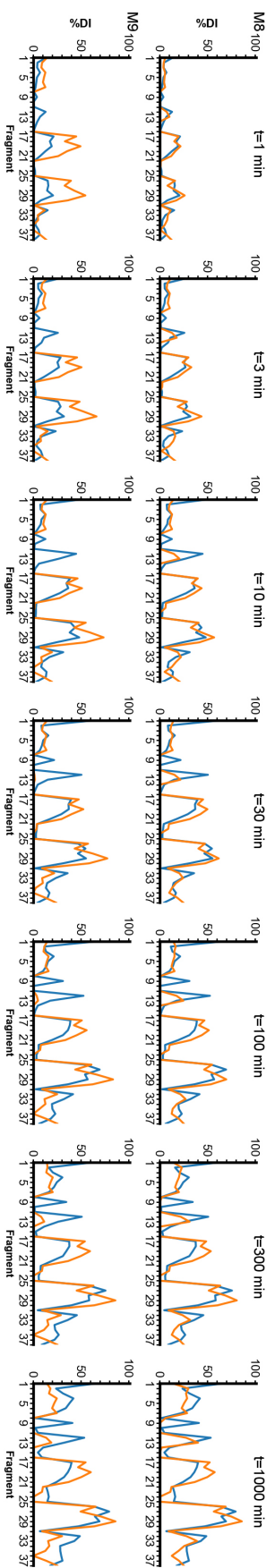


Figure S15: Deuterium incorporation of fragments in RGS8. The HDX experiment (blue) and the new models (M8, M9) with optimized parameters (red) are shown in seven discrete times. This figure shows the MD simulation results for PDB:2IHD and AMBER Force-field.

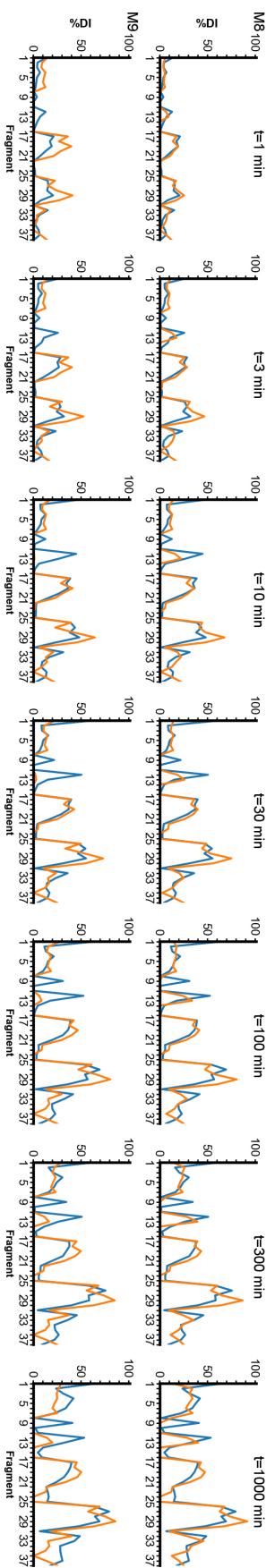


Figure S16: Deuterium incorporation of fragments in RGS8. The HDX experiment (blue) and the new models (M8, M9) with optimized parameters (red) are shown in seven discrete times. This figure shows the MD simulation results for PDB:2ODE and AMBER Force-field.

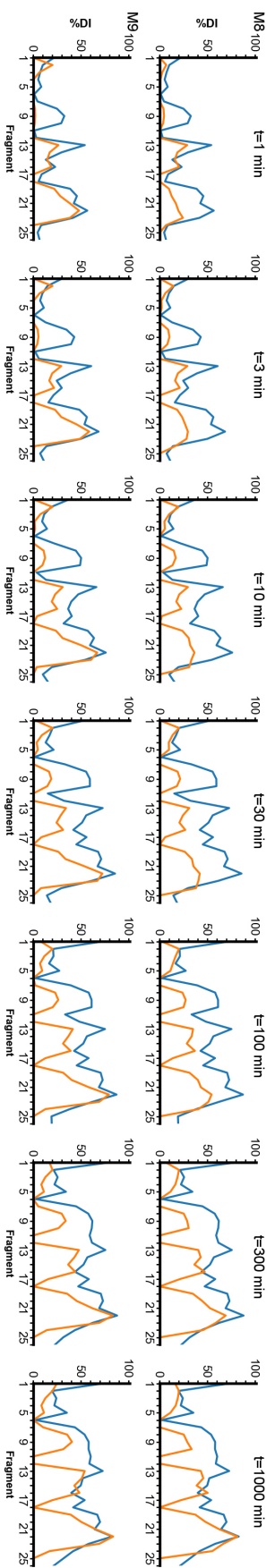


Figure S17: Deuterium incorporation of fragments in RGS19. The HDX experiment (blue) and the new models (M8, M9) with optimized parameters (red) are shown in seven discrete times. This figure shows the MD simulation results for PDB: 1CMZ and AMBER Force-field.

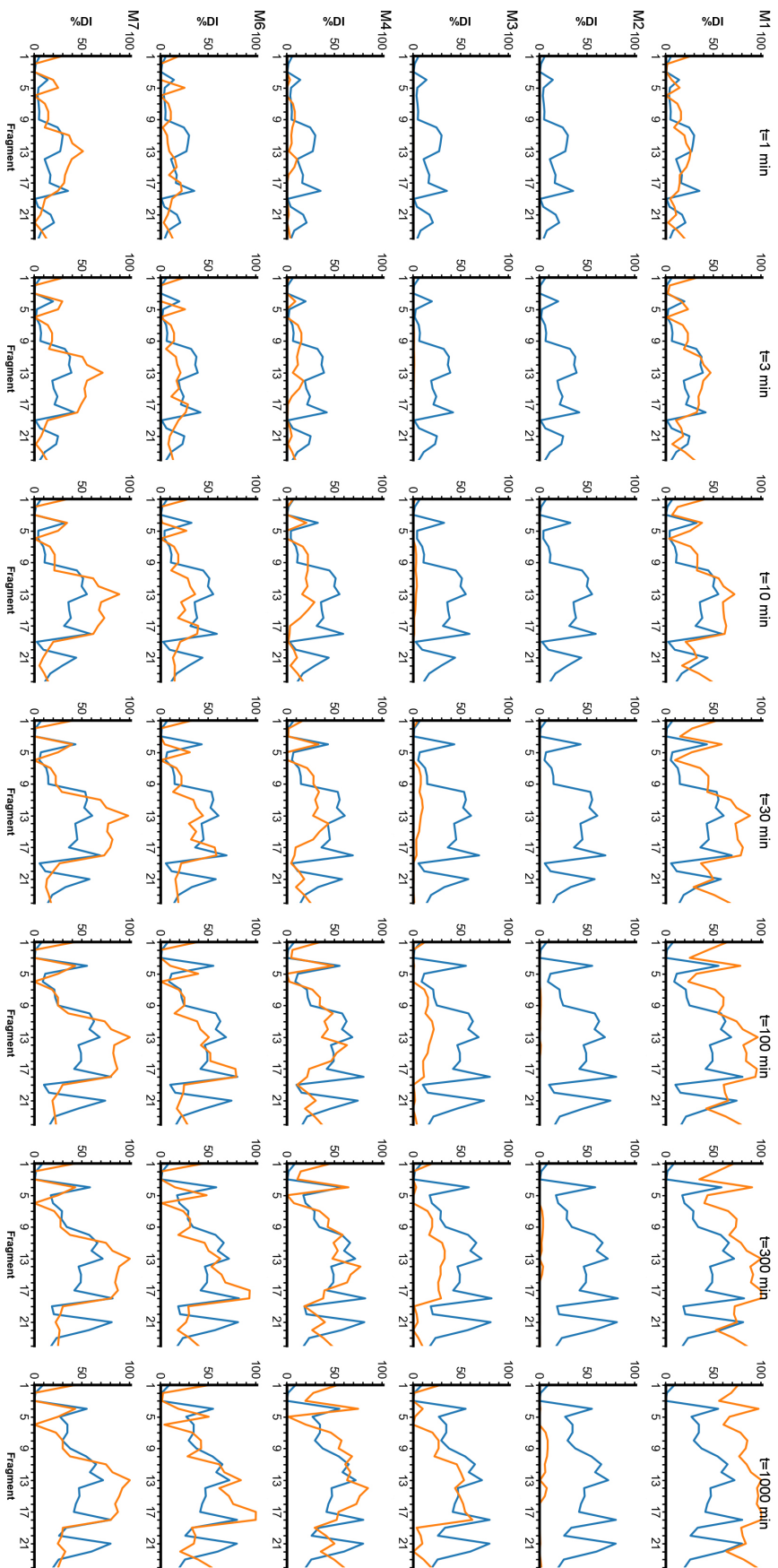


Figure S18: Deuterium incorporation of fragments in RGS4. The HDX experiment (blue) and different models with default parameters (red) are shown in seven discrete times. This figure shows the MD simulation results for PDB:1AGR and CHARMM Force-field.

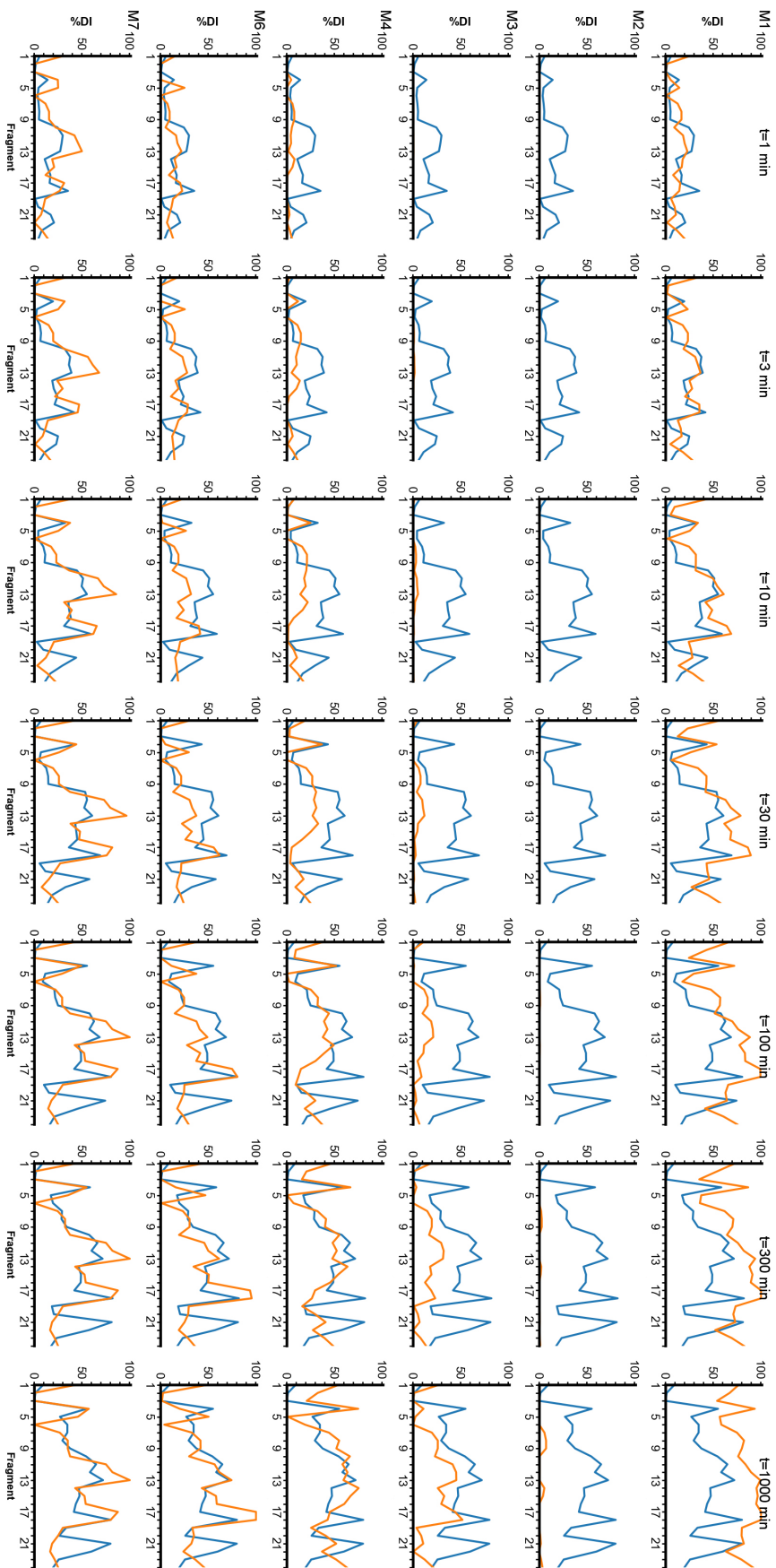


Figure S19: Deuterium incorporation of fragments in RGS4. The HDX experiment (blue) and different models with default parameters (red) are shown in seven discrete times. This figure shows the MD simulation results for PDB:1E7T and CHARMM Force-field.

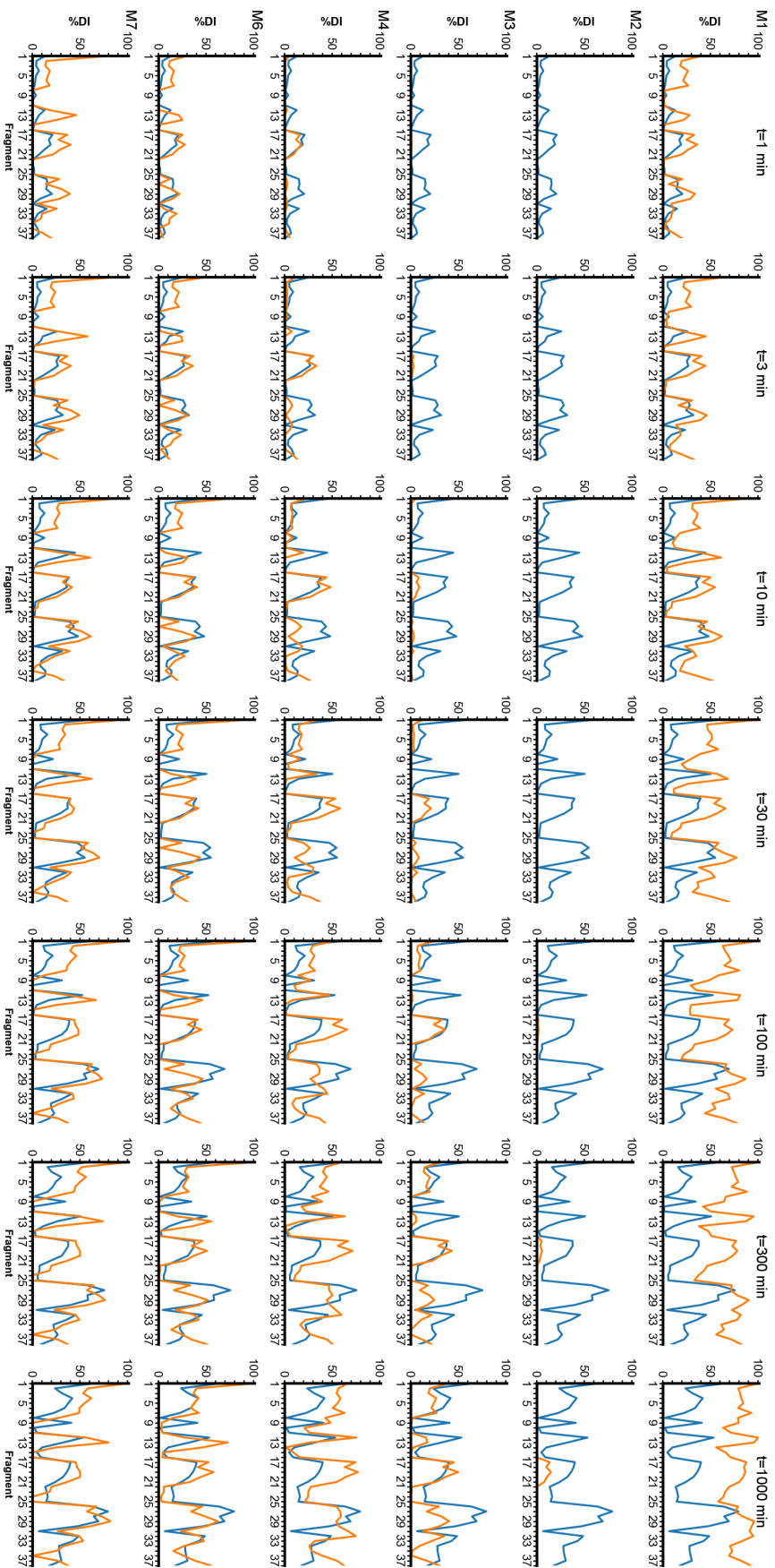


Figure S20: Deuterium incorporation of fragments in RGS8. The HDX experiment (blue) and different models with default parameters (red) are shown in seven discrete times. This figure shows the MD simulation results for PDB:2IHD and CHARMM Force-field.

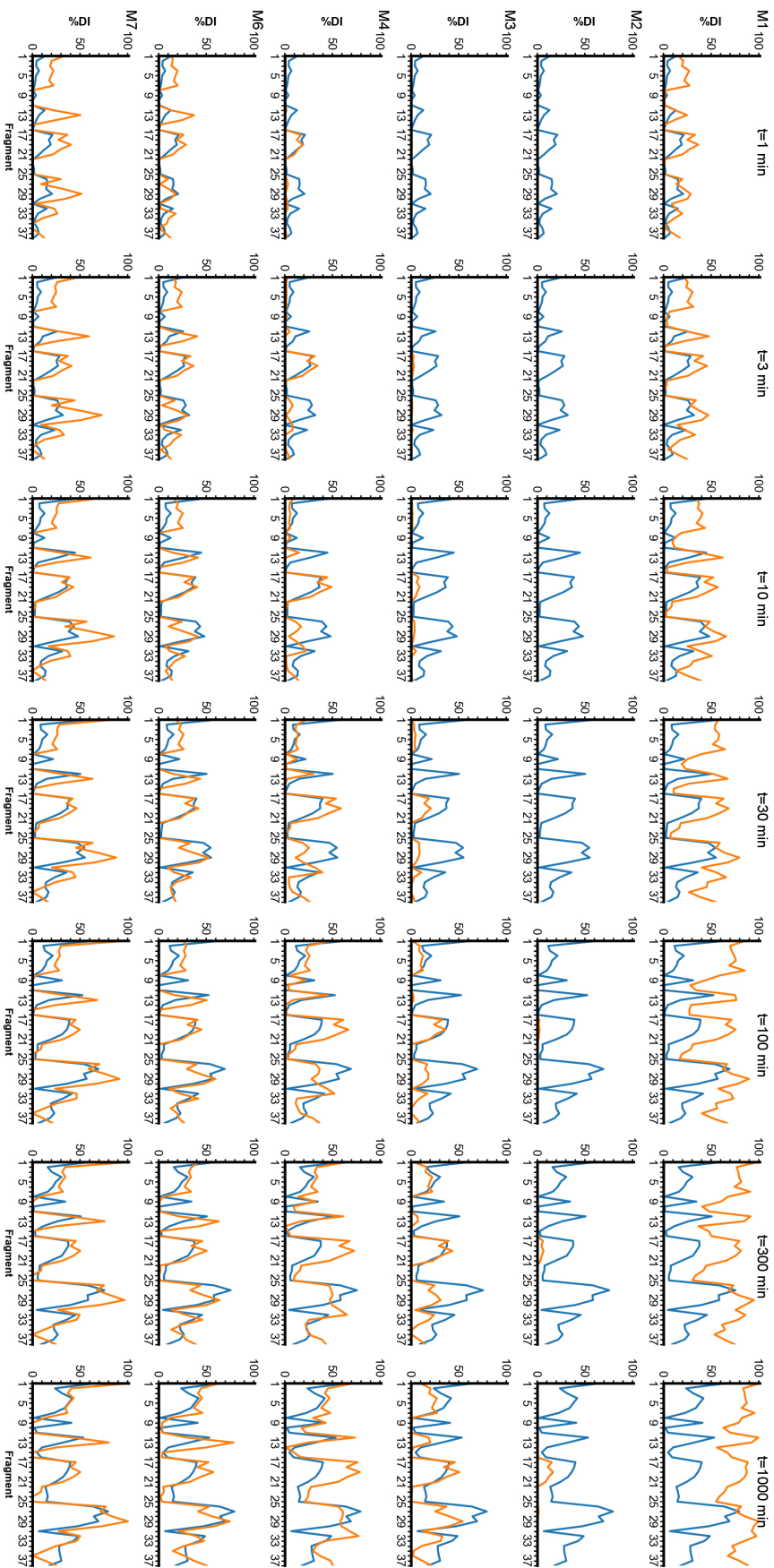


Figure S21: Deuterium incorporation of fragments in RGS8. The HDX experiment (blue) and different models with default parameters (red) are shown in seven discrete times. This figure shows the MD simulation results for PDB:2ODE and CHARMM Force-field.



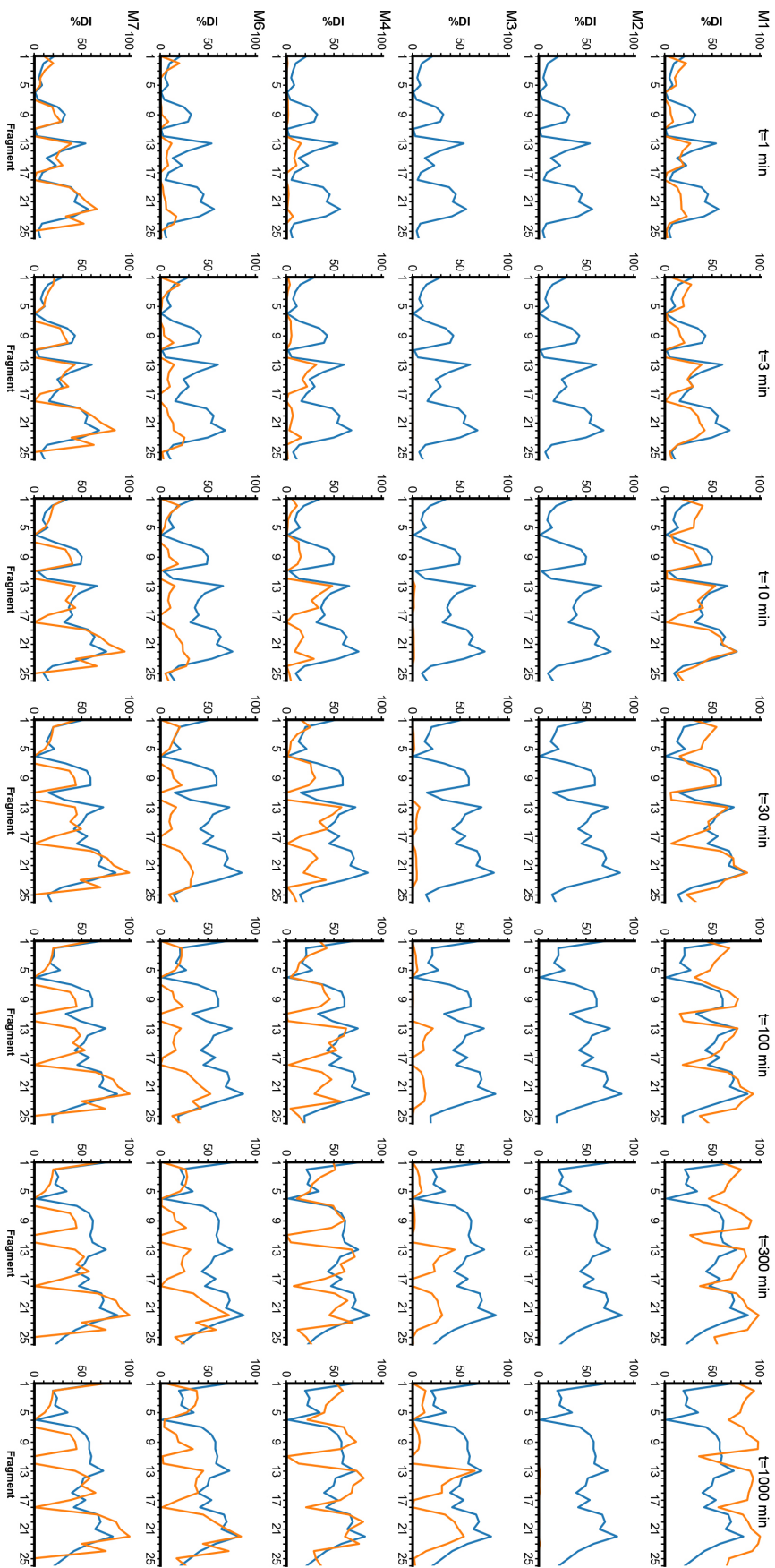


Figure S22: Deuterium incorporation of fragments in RGS19. The HDX experiment (blue) and different models with default parameters (red) are shown in seven discrete times. This figure shows the MD simulation results for PDB:1CMZ and CHARMM Force-field.

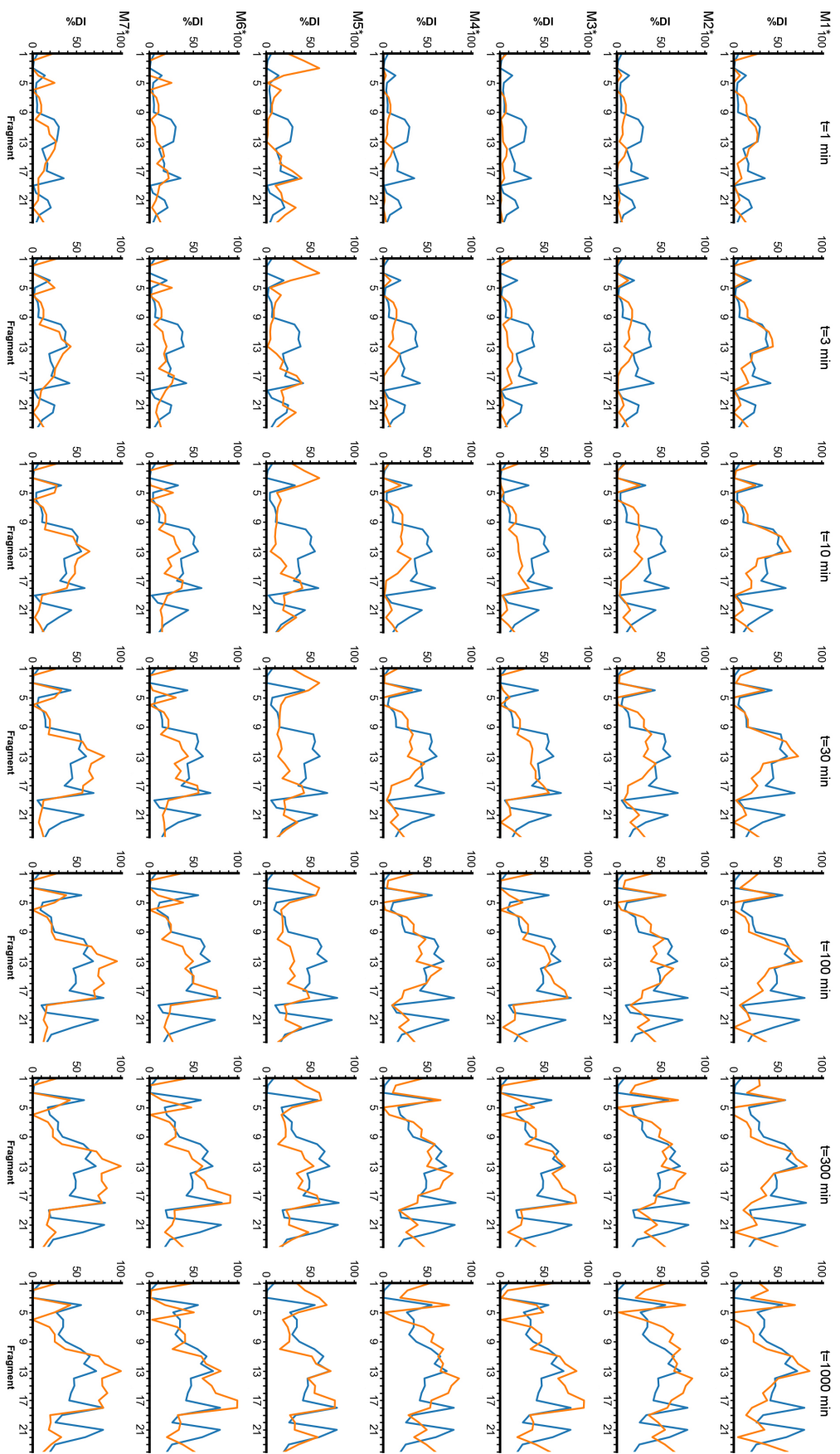


Figure S23: Deuterium incorporation of fragments in RGS4. The HDX experiment (blue) and different models with optimized parameters (red) are shown in seven discrete times. This figure shows the MD simulation results for PDB:1AGR and CHARMM Force-field.

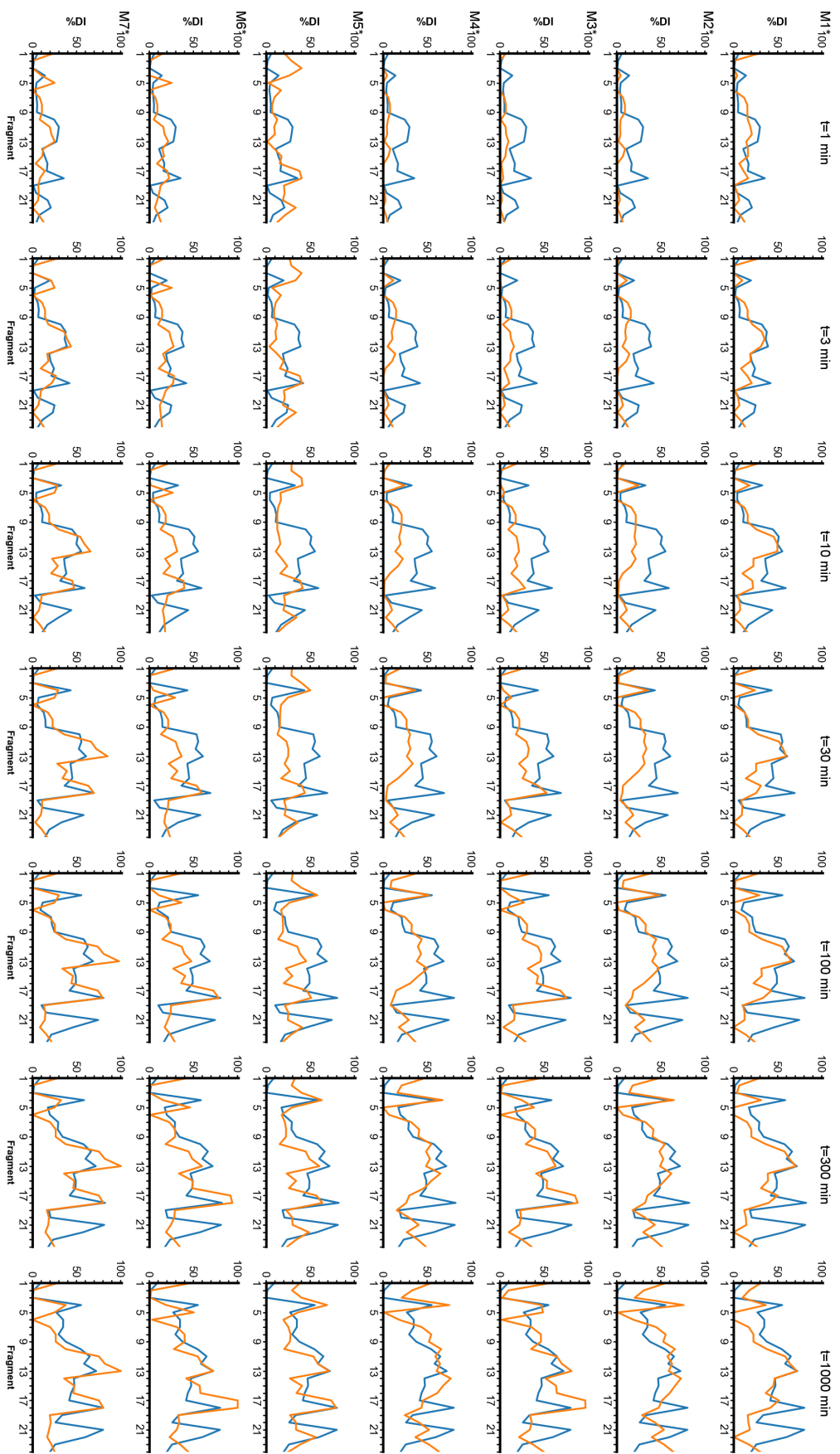


Figure S24: Deuterium incorporation of fragments in RGS4. The HDX experiment (blue) and different models with optimized parameters (red) are shown in seven discrete times. This figure shows the MD simulation results for PDB:1E7T and CHARMM Force-field.

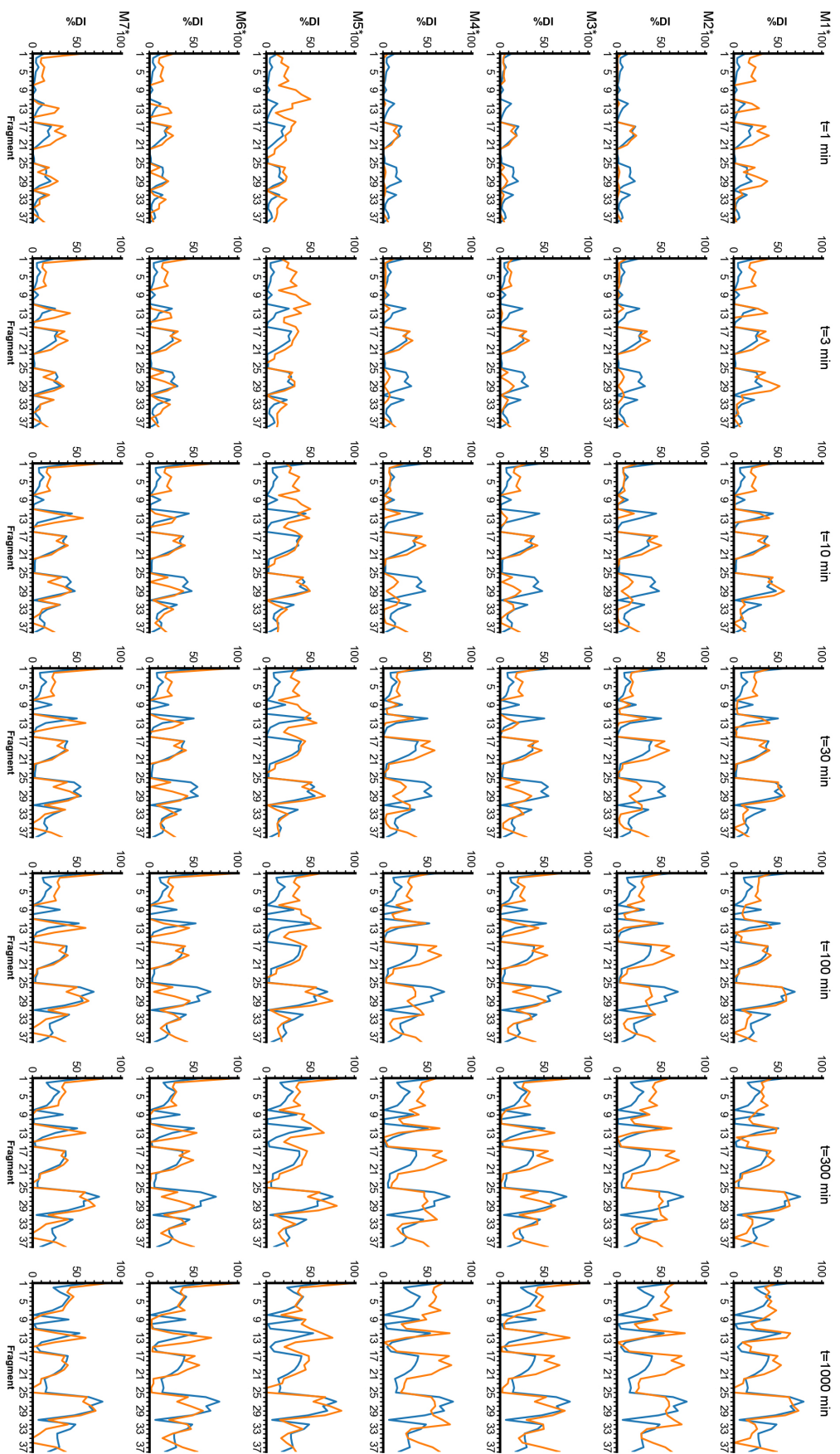


Figure S25: Deuterium incorporation of fragments in RGS8. The HDX experiment (blue) and different models with optimized parameters (red) are shown in seven discrete times. This figure shows the MD simulation results for PDB:2IHD and CHARMM Force-field.

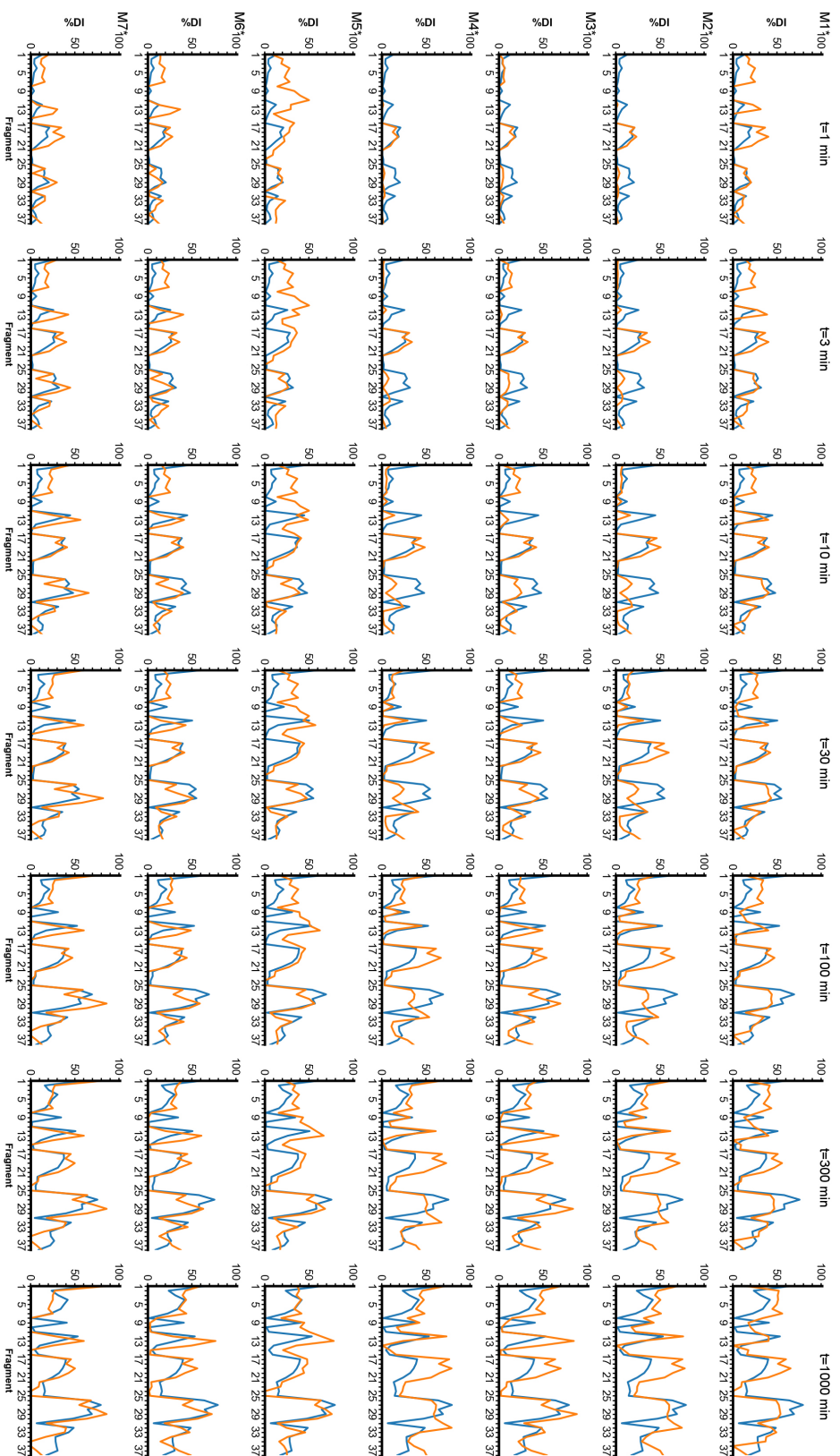


Figure S26: Deuterium incorporation of fragments in RGS8. The HDX experiment (blue) and different models with optimized parameters (red) are shown in seven discrete times. This figure shows the MD simulation results for PDB:2ODE and CHARMM Force-field.

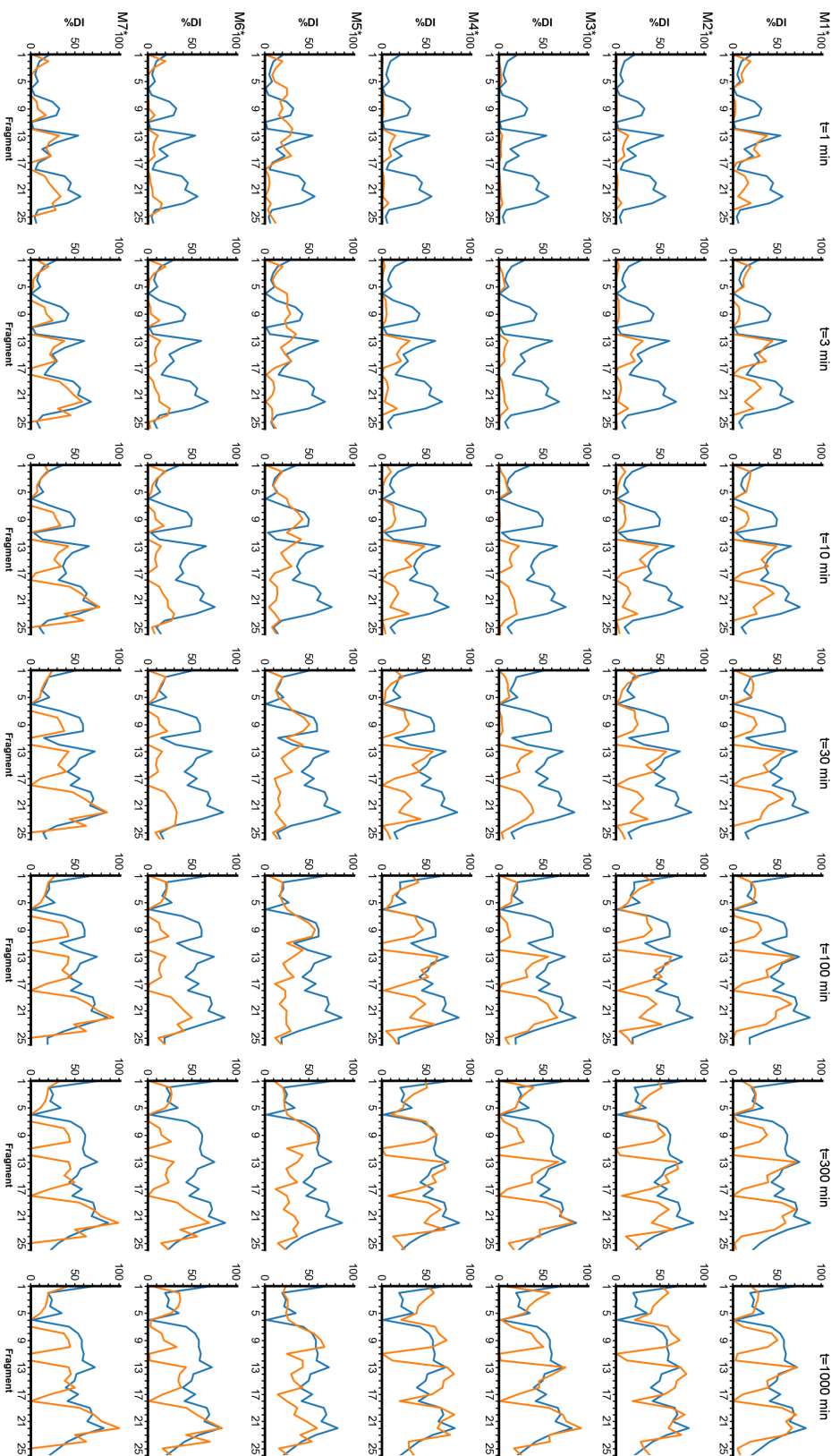


Figure S27: Deuterium incorporation of fragments in RGS19. The HDX experiment (blue) and different models with optimized parameters (red) are shown in seven discrete times. This figure shows the MD simulation results for PDB:1CMZ and CHARMM Force-field.

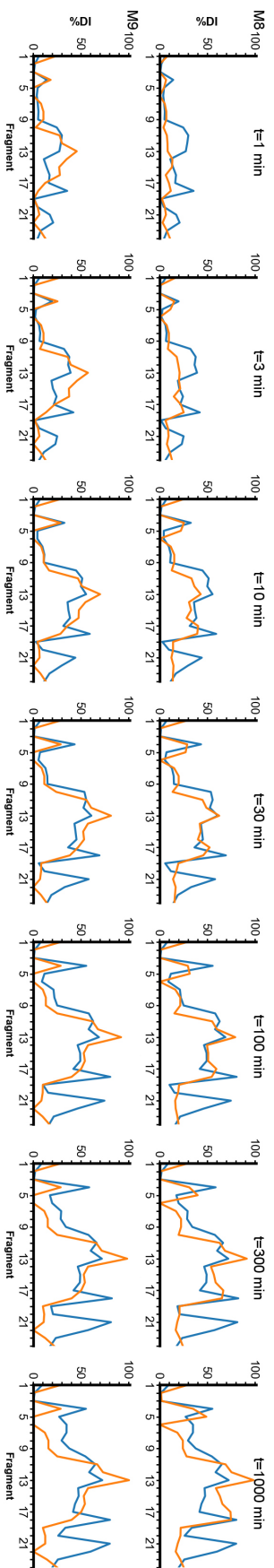


Figure S28: Deuterium incorporation of fragments in RGS4. The HDX experiment (blue) and the new models (M8, M9) with optimized parameters (red) are shown in seven discrete times. This figure shows the MD simulation results for PDB:1AGR and CHARMM Force-field.

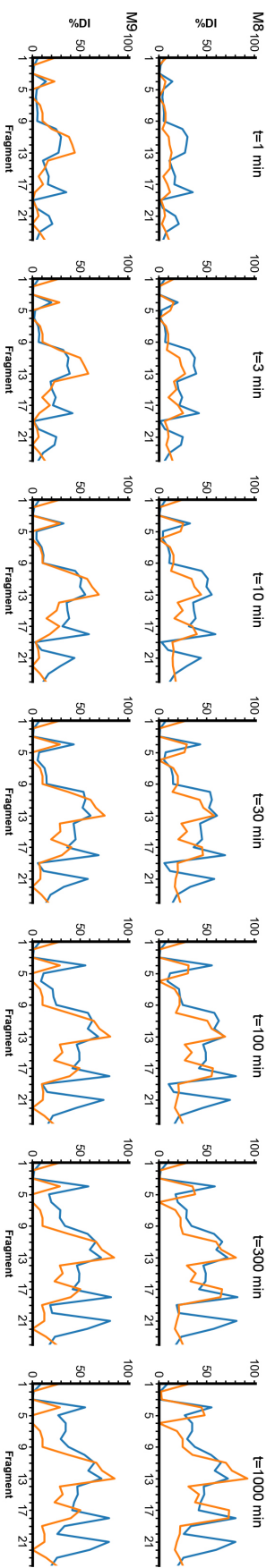


Figure S29: Deuterium incorporation of fragments in RGS4. The HDX experiment (blue) and the new models (M8, M9) with optimized parameters (red) are shown in seven discrete times. This figure shows the MD simulation results for PDB:IEZT and CHARMM Force-field.



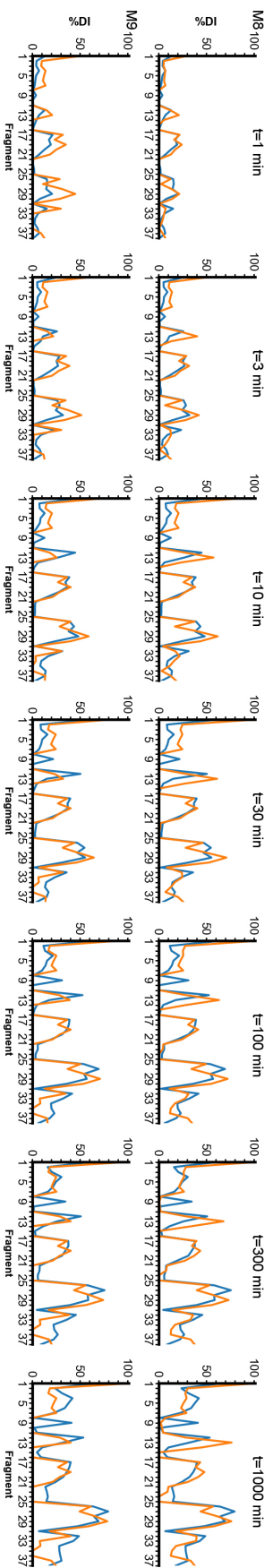


Figure S30: Deuterium incorporation of fragments in RGS8. The HDX experiment (blue) and the new models (M8, M9) with optimized parameters (red) are shown in seven discrete times. This figure shows the MD simulation results for PDB:2IHD and CHARMM Force-field.

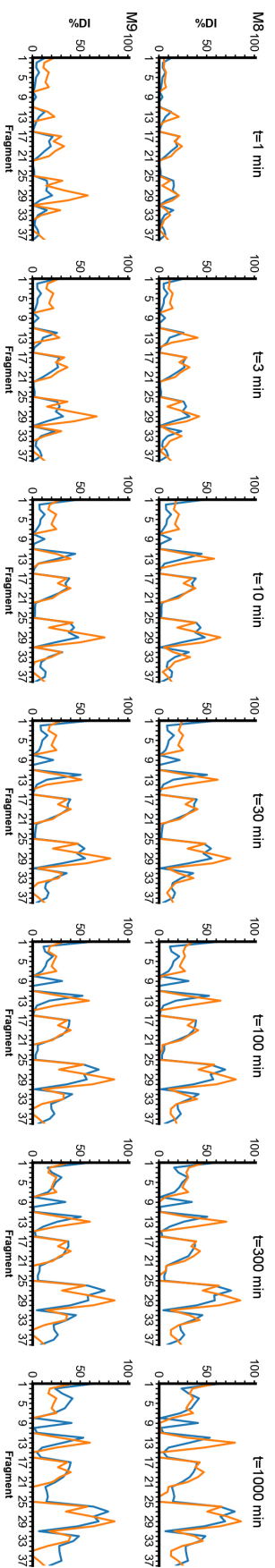


Figure S31: Deuterium incorporation of fragments in RGS8. The HDX experiment (blue) and the new models (M8, M9) with optimized parameters (red) are shown in seven discrete times. This figure shows the MD simulation results for PDB:2ODE and CHARMM Force-field.

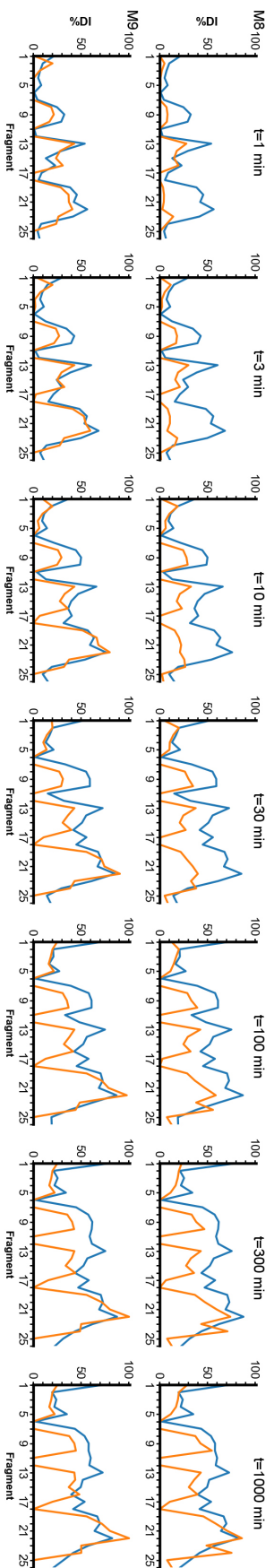


Figure S32: Deuterium incorporation of fragments in RGS19. The HDX experiment (blue) and the new models (M8, M9) with optimized parameters (red) are shown in seven discrete times. This figure shows the MD simulation results for PDB:1CMZ and CHARMM Force-field.

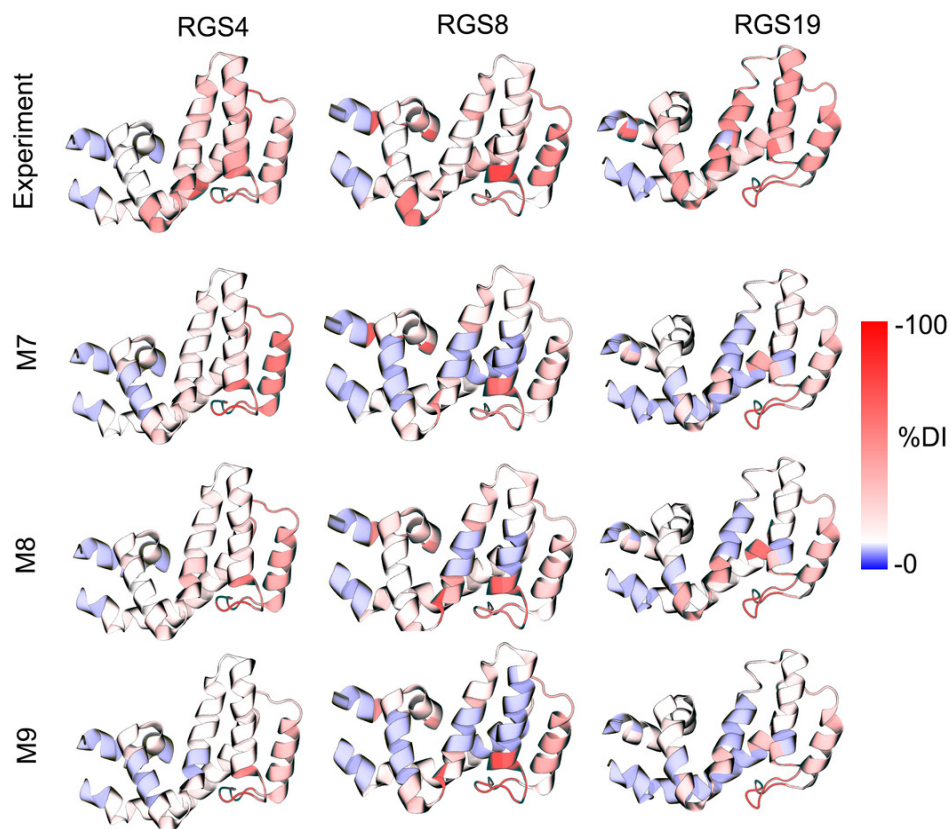


Figure S33: Deuterium incorporation is mapped on RGS proteins at  $t = 1000$  min as observed in experiments and as predicted by the models M7, M8, and M9. Data are presented for the CHARMM-FF simulations of RGS4, RGS8, and RGS19.

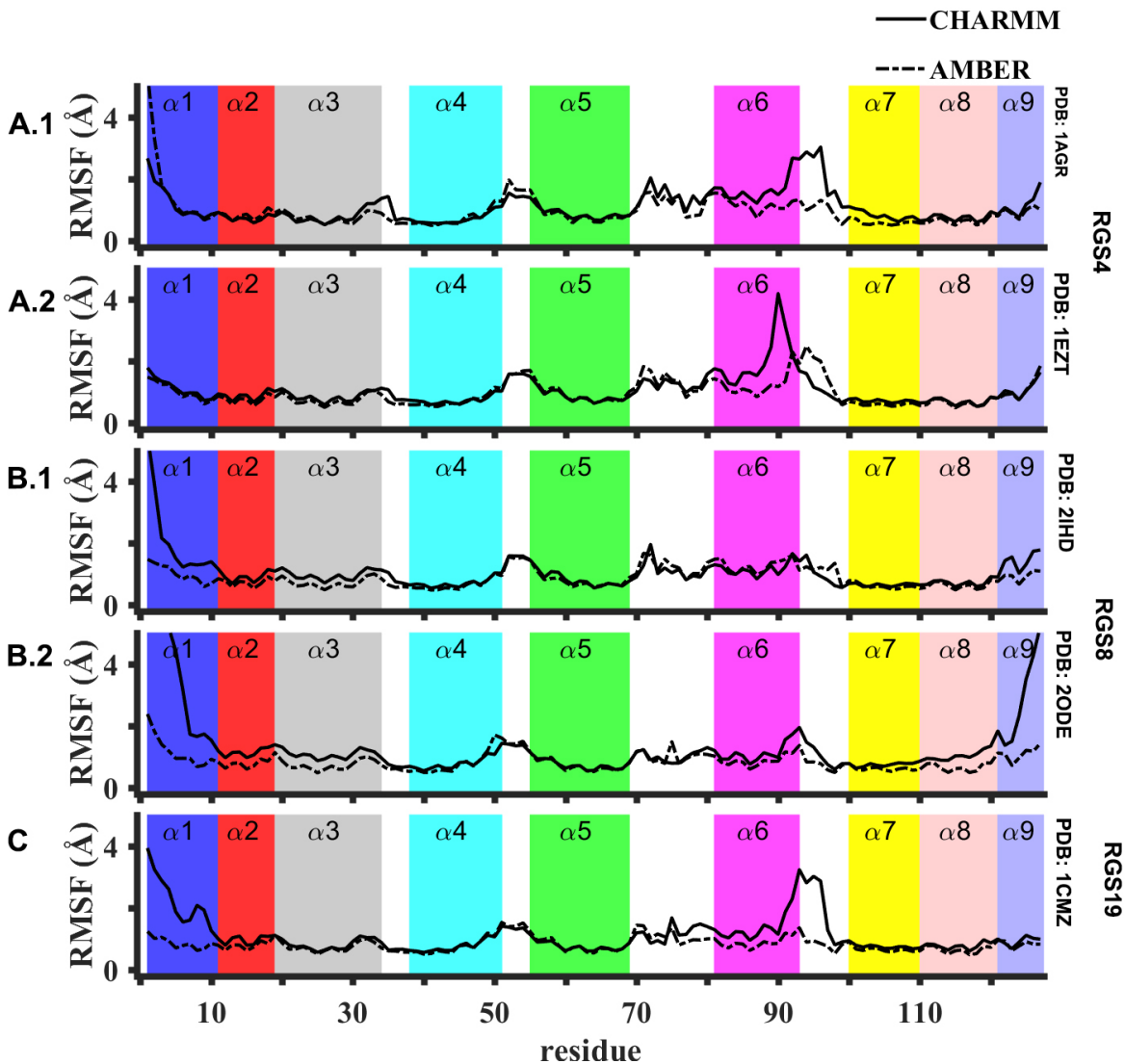


Figure S34: Root mean squared fluctuations (RMSF) per residue across protein sequences are shown from 2- $\mu$ s long MD simulations of (A) RGS4 (PDB: 1AGR, 1EZT), (B) RGS8 (PDB: 2IHD, 2ODE), and (C) RGS19 (PDB: 1CMZ). Color bars indicate helical regions.

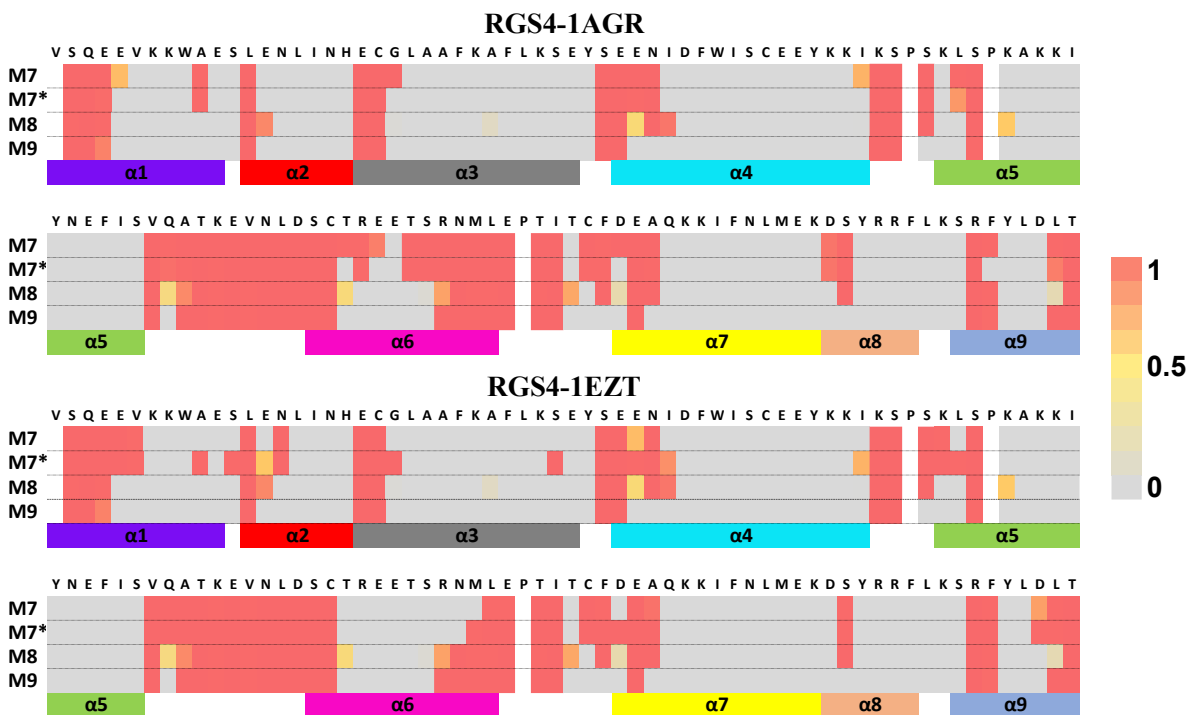


Figure S35: Modeled deuterium incorporation at  $t = 1000$  min at a single-residue resolution (RGS4, CHARMM-FF).

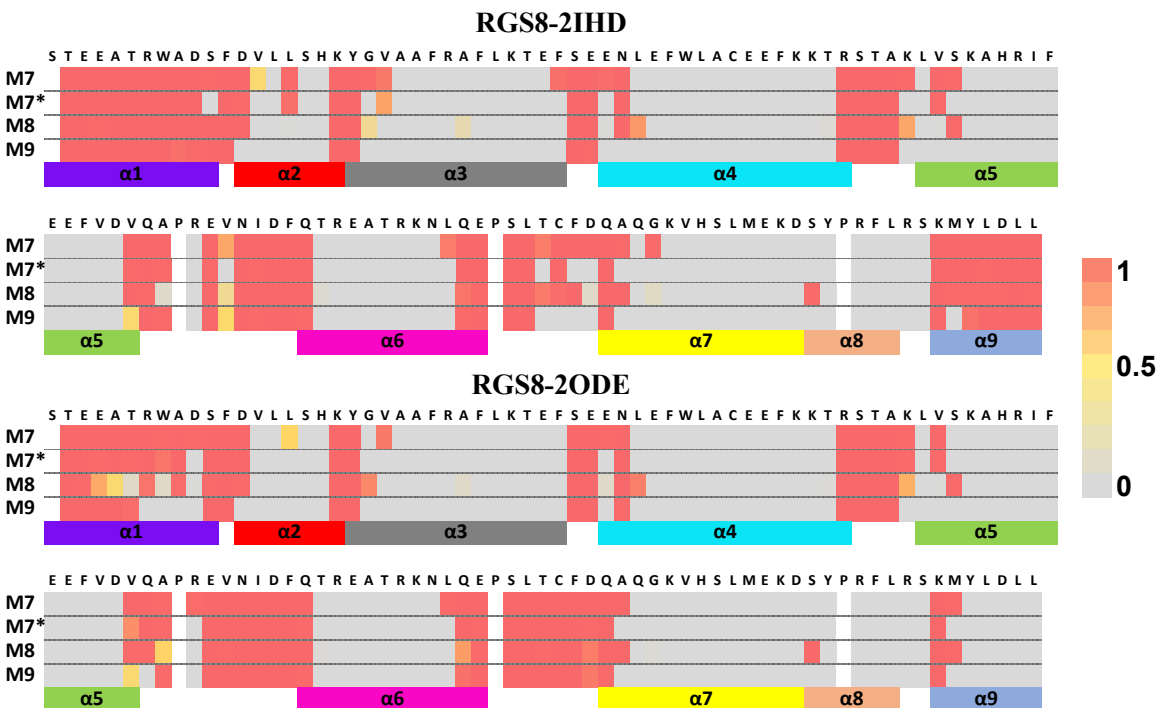


Figure S36: Modeled deuterium incorporation at  $t = 1000$  min at a single-residue resolution (RGS8, CHARMM-FF).

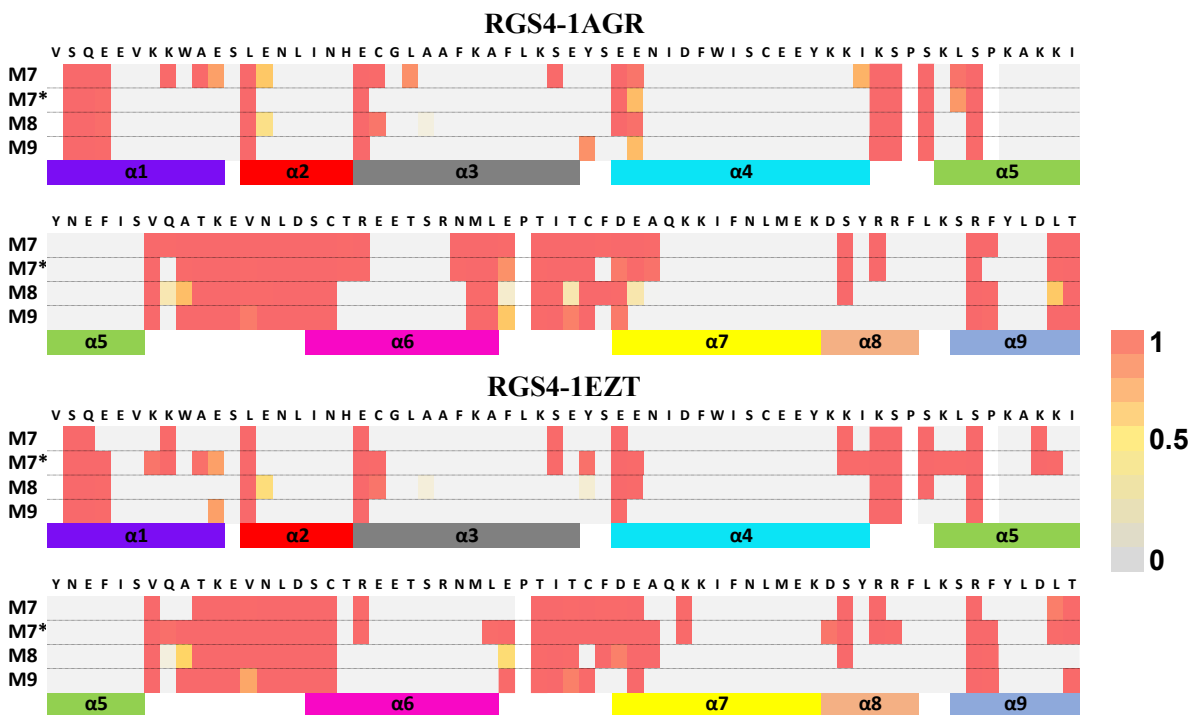


Figure S37: Modeled deuterium incorporation at  $t = 1000$  min at a single-residue resolution (RGS4, AMBER-FF).

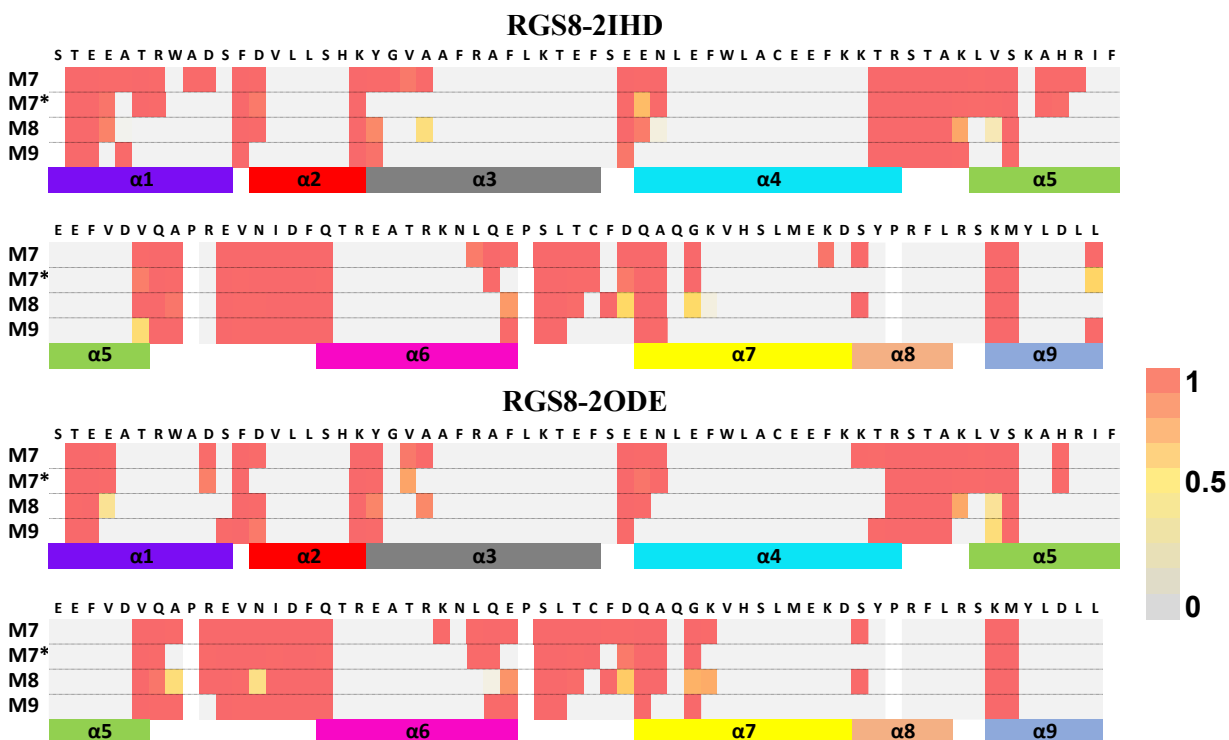


Figure S38: Modeled deuterium incorporation at  $t = 1000$  min at a single-residue resolution (RGS8, AMBER-FF).

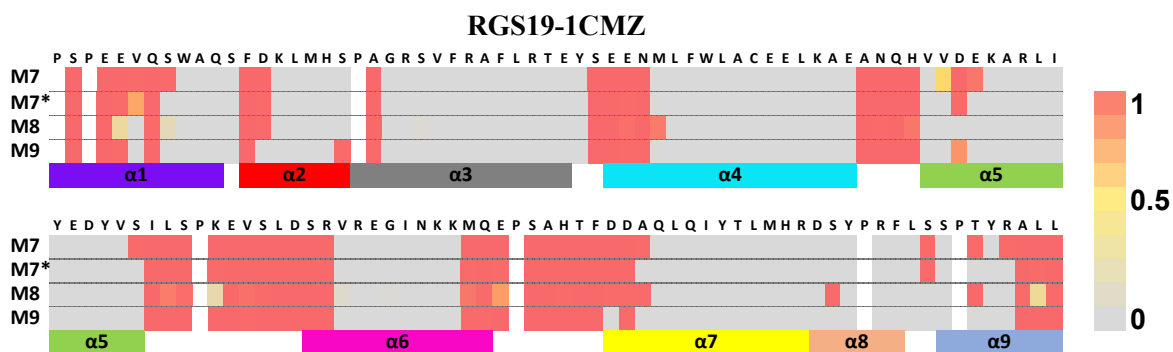


Figure S39: Modeled deuterium incorporation at  $t = 1000$  min at a single-residue resolution (RGS19, CHARMM-FF).

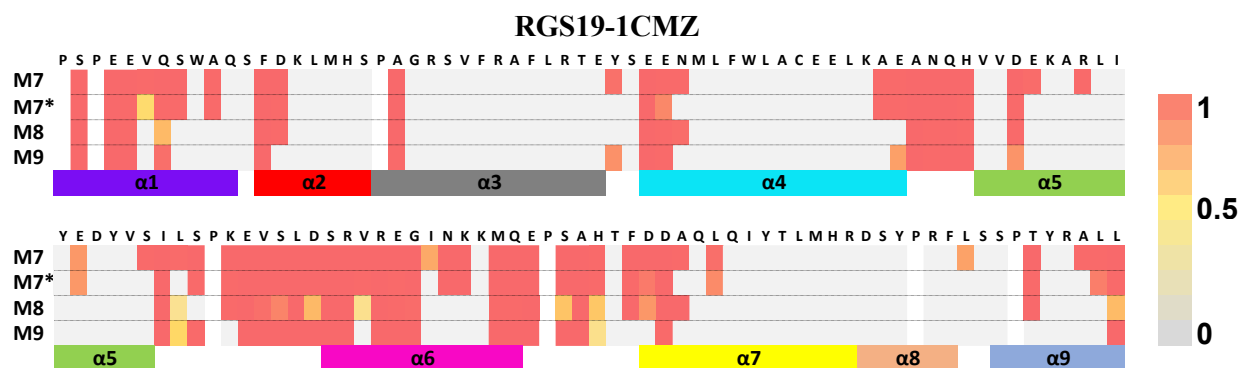


Figure S40: Modeled deuterium incorporation at  $t = 1000$  min at a single-residue resolution (RGS19, AMBER-FF).



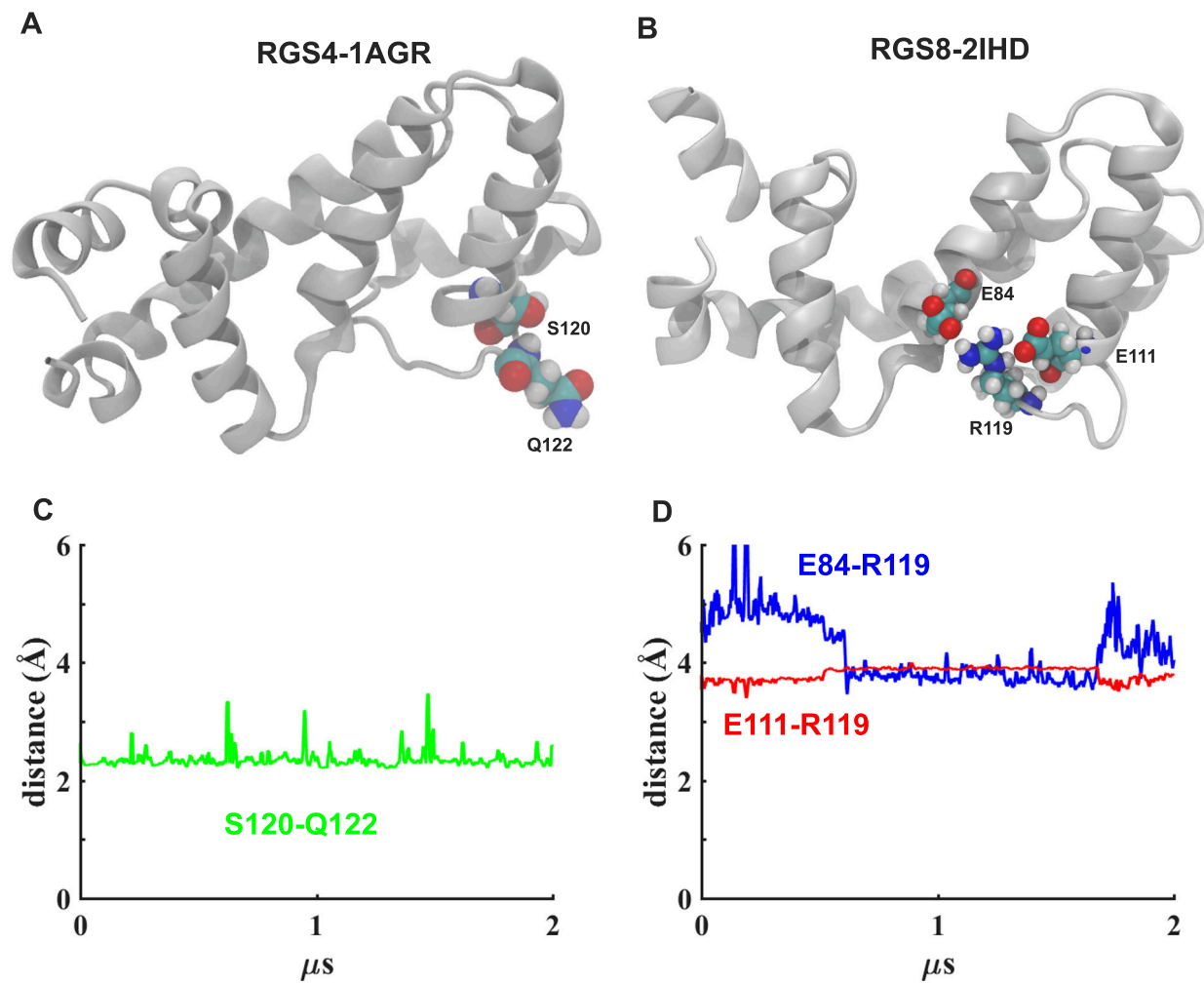


Figure S41: The residues protected by hydrogen-bonds or salt-bridging interactions are highlighted (panels A and B). The traces for distances between the centers-of-masses of residue pairs are shown in panel C (S120-Q122) and panel D (E84-R119 and E111-R119).

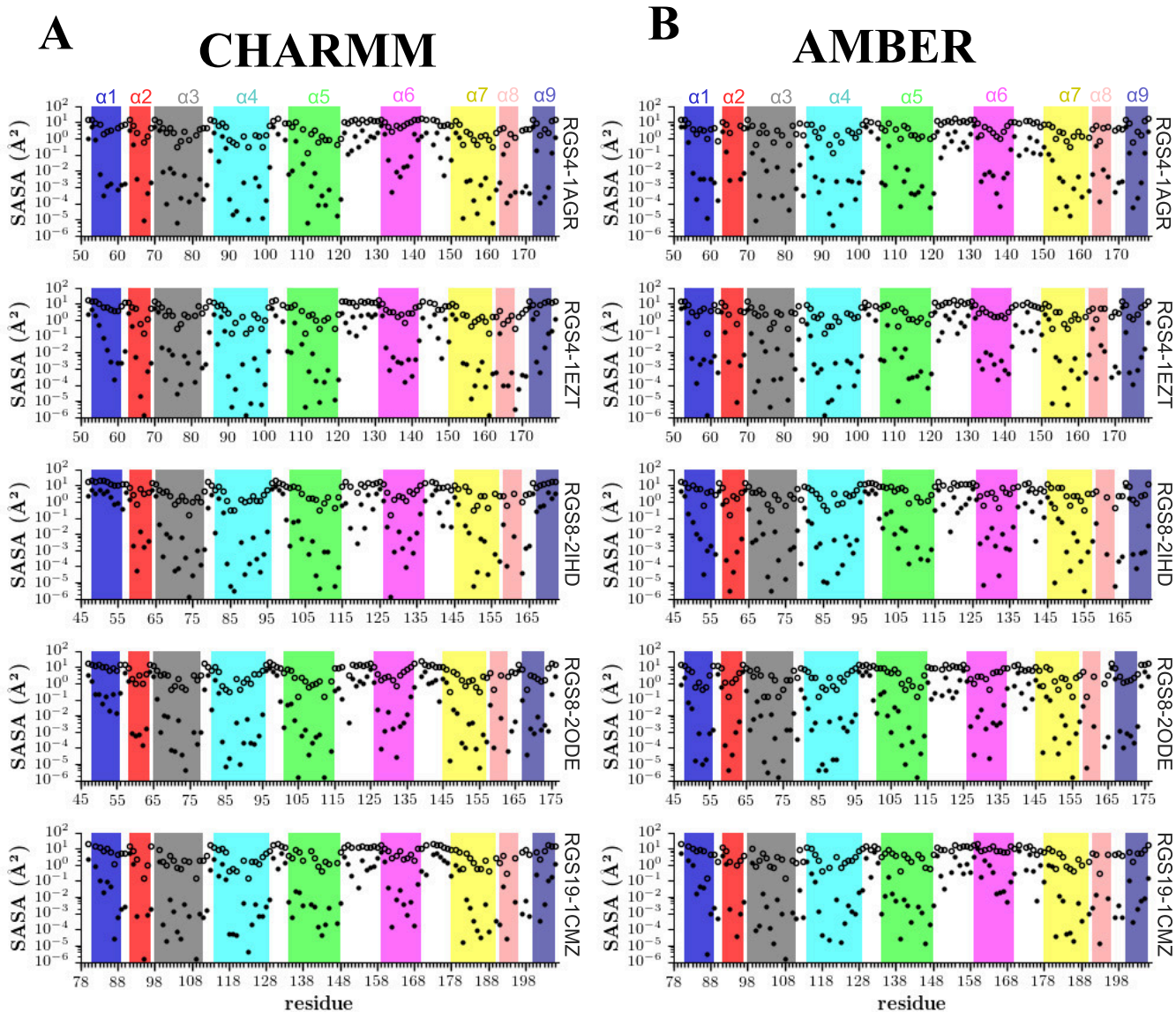


Figure S42: SASA data similar to Figure 5 are shown from MD simulations of all RGS proteins for both force-fields (CHARMM-FF, panel A; AMBER-FF, panel B). Color and labeling details are similar to Figure 5.

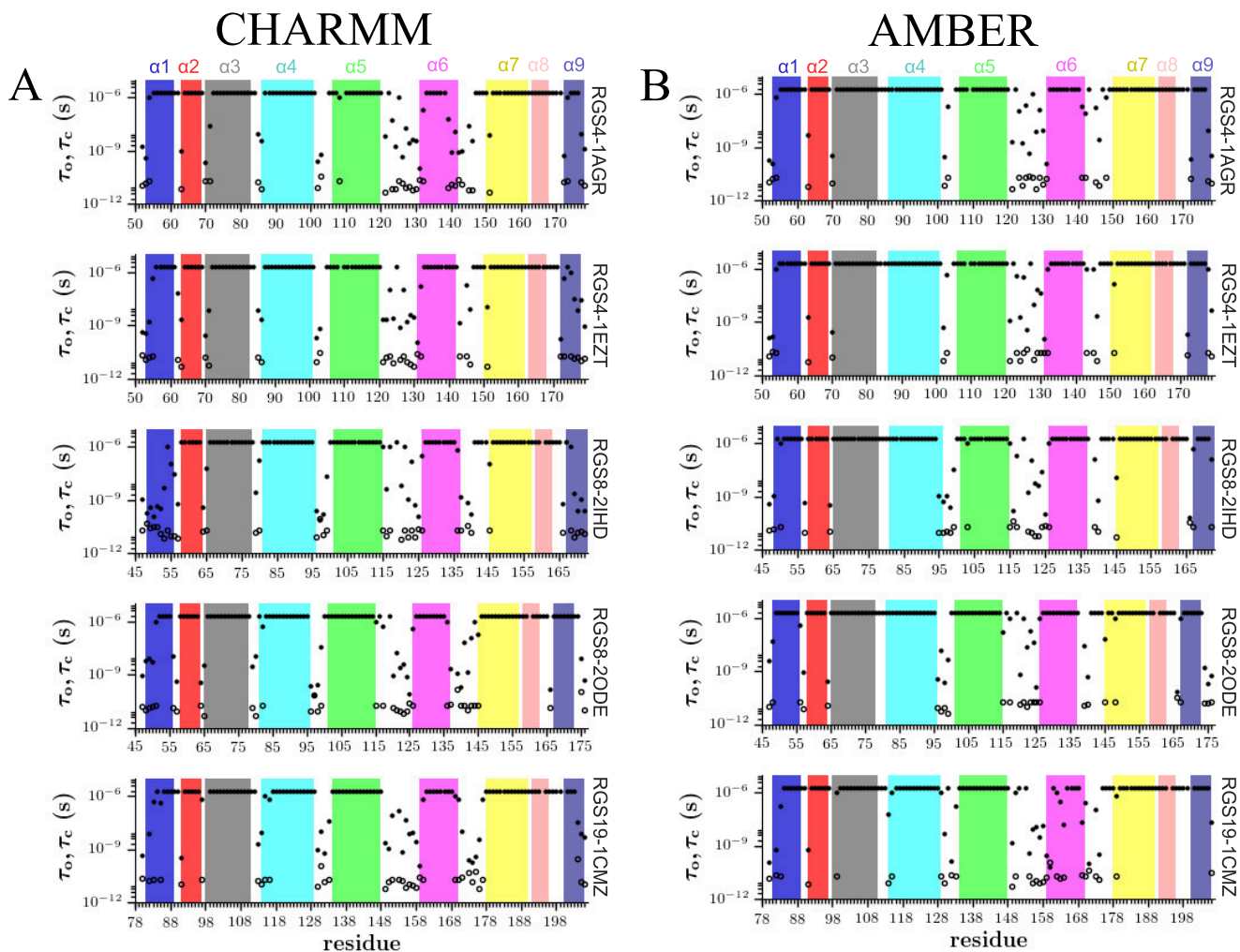


Figure S43: Corrected mean residence times for open-states of amide hydrogens are shown. Other details are similar to Figure 6.



Figure S44: Residue-residue correlations among open states of all amide-hydrogens (CHARMM-FF, RGS4 (PDB code 1AGR), model M7). The correlation matrix is calculated based on the probability that two amide-hydrogens simultaneously explore open states;  $C(i, j) = (P(i, j) - P(i)P(j)) / (P(i)P(j)(1 - P(i))(1 - P(j)))^{0.5}$ .<sup>9</sup>



Figure S45: Data similar to Figure S44 are shown for RGS8 (CHARMM-FF, RGS8 (PDB code 2ODE), model M7).<sup>9</sup>

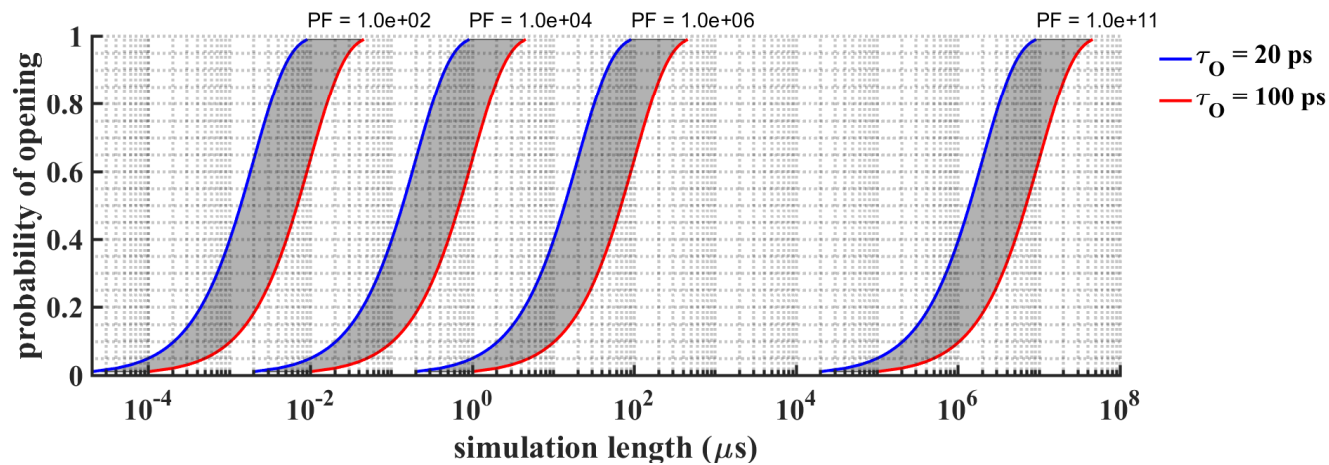


Figure S46: Probability of a closed to open transition in a given amide vs. simulation length ( $\mu\text{s}$ ) is presented based upon Poisson statistics.<sup>9</sup> Data are shown for PFs =  $10^2$ ,  $10^4$ ,  $10^6$ , and  $10^{11}$  with  $\tau_O = 20 \text{ ps}$  and  $100 \text{ ps}$ .

## References

- [1] Resing, K. A.; Hoofnagle, A. N.; Ahn, N. G. Modeling deuterium exchange behavior of ERK2 using pepsin mapping to probe secondary structure. *J. Am. Soc. Mass. Spectrom.* **1999**, *10*, 685–702.
- [2] Bai, Y.; Milne, J. S.; Mayne, L.; Englander, S. W. Primary structure effects on peptide group hydrogen exchange. *Proteins* **1993**, *17*, 75–86.
- [3] Milne, J.; Mayne, L.; Roder, H.; Wand, A.; Englander, S. Determinants of protein hydrogen exchange studied in equine cytochrome c. *Protein Sci.* **1998**, *7*, 739–745.
- [4] Vendruscolo, M.; Paci, E.; Dobson, C. M.; Karplus, M. Rare fluctuations of native proteins sampled by equilibrium hydrogen exchange. *J. Am. Chem. Soc.* **2003**, *125*, 15686–15687.
- [5] Best, R. B.; Vendruscolo, M. Structural interpretation of hydrogen exchange protection factors in proteins: characterization of the native state fluctuations of CI2. *Structure* **2006**, *14*, 97–106.
- [6] Kieseritzky, G.; Morra, G.; Knapp, E.-W. Stability and fluctuations of amide hydrogen bonds in a bacterial cytochrome c: a molecular dynamics study. *J. Biol. Inorg. Chem.* **2006**, *11*, 26–40.
- [7] Ma, B.; Nussinov, R. Polymorphic triple  $\beta$ -sheet structures contribute to amide hydrogen/deuterium (H/D) exchange protection in the Alzheimer amyloid  $\beta$ 42 peptide. *J. Biol. Chem.* **2011**, *286*, 34244–34253.
- [8] Park, I.-H.; Venable, J. D.; Steckler, C.; Cellitti, S. E.; Lesley, S. A.; Spraggon, G.; Brock, A. Estimation of hydrogen-exchange protection factors from MD simulation based on amide hydrogen bonding analysis. *J. Chem. Inf. Model.* **2015**, *55*, 1914–1925.
- [9] Persson, F.; Halle, B. How amide hydrogens exchange in native proteins. *Proc. Natl. Sci. Acad. USA* **2015**, *112*, 10383–10388.

- [10] Shaw, D. E.; Maragakis, P.; Lindorff-Larsen, K.; Piana, S.; Dror, R. O.; Eastwood, M. P.; Bank, J. A.; Jumper, J. M.; Salmon, J. K.; Shan, Y.; Wriggers, W. Atomic-level characterization of the structural dynamics of proteins. *Science* **2010**, *330*, 341–346.
- [11] Craig, P. O.; Lätzer, J.; Weinkam, P.; Hoffman, R. M.; Ferreiro, D. U.; Komives, E. A.; Wolynes, P. G. Prediction of native-state hydrogen exchange from perfectly funneled energy landscapes. *J. Am. Chem. Soc.* **2011**, *133*, 17463–17472.
- [12] Petruk, A. A.; Defelipe, L. A.; Rodríguez Limardo, R. G.; Bucci, H.; Marti, M. A.; Turjanski, A. G. Molecular dynamics simulations provide atomistic insight into hydrogen exchange mass spectrometry experiments. *J. Chem. Theory Comput.* **2012**, *9*, 658–669.
- [13] Adhikary, S.; Deredge, D. J.; Nagarajan, A.; Forrest, L. R.; Wintrose, P. L.; Singh, S. K. Conformational dynamics of a neurotransmitter: sodium symporter in a lipid bilayer. *Proc. Natl. Sci. Acad. USA* **2017**, *114*, E1786–E1795.
- [14] McAllister, R. G.; Konermann, L. Challenges in the interpretation of protein H/D exchange data: a molecular dynamics simulation perspective. *Biochemistry* **2015**, *54*, 2683–2692.
- [15] Maity, H.; Lim, W. K.; Rumbley, J. N.; Englander, S. W. Protein hydrogen exchange mechanism: local fluctuations. *Protein Sci.* **2003**, *12*, 153–160.